

April 2015

Design and Fabrication of a Radio-Frequency Electrothermal Thruster

Ryan James Byrne
Worcester Polytechnic Institute

Scott David Osborn
Worcester Polytechnic Institute

Zackary Philip Tripp
Worcester Polytechnic Institute

Follow this and additional works at: <https://digitalcommons.wpi.edu/mqp-all>

Repository Citation

Byrne, R. J., Osborn, S. D., & Tripp, Z. P. (2015). *Design and Fabrication of a Radio-Frequency Electrothermal Thruster*. Retrieved from <https://digitalcommons.wpi.edu/mqp-all/2280>

This Unrestricted is brought to you for free and open access by the Major Qualifying Projects at Digital WPI. It has been accepted for inclusion in Major Qualifying Projects (All Years) by an authorized administrator of Digital WPI. For more information, please contact digitalwpi@wpi.edu.

Design and Fabrication of a Radio-Frequency Electrothermal Thruster

A Major Qualifying Project Report

Submitted to the Faculty of the

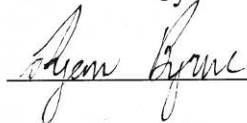
WORCESTER POLYTECHNIC INSTITUTE

in Partial Fulfillment of the Requirements for the

Degree of Bachelor of Science

in Aerospace Engineering

by



Ryan Byrne



Scott Osborn



Zackary Tripp

April 30, 2015

Approved by:



Professor John J. Blandino, Advisor
Aerospace Engineering Program
Mechanical Engineering Department, WPI

Table of Contents

ABSTRACT	3
LIST OF TABLES	6
ACKNOWLEDGEMENTS	7
TABLE OF AUTHORSHIP	8
CHAPTER 1: INTRODUCTION	9
CHAPTER 2: BACKGROUND	11
2.1 Radio Frequency Discharges	11
2.1.1 Plasma Basics	11
2.1.2 Plasma Generation.....	12
2.1.3 E and H Mode.....	14
2.2 Radio Frequency Electrothermal Thrusters (RFET)	15
2.2.1 Principles of Operation	15
2.2.2 Pennsylvania State University RFET	17
2.2.3 Pocket Rocket RFET.....	19
2.2.4 Variable Length RFET	20
2.3 Vacuum System Technology	21
2.3.1 Need for a Vacuum	21
2.3.2 Vacuum Pumps	22
2.3.3 Vacuum Measurements.....	25
2.4 Optical Spectroscopy.....	26
2.4.1 General Principles	26
2.4.2 Previous Spectroscopic Studies of RFET Thrusters	27
2.4.3 Visual Characteristics of Argon	29
2.5 Impedance Matching Networks.....	29
2.5.1 Importance of Impedance Matching Networks	29
2.5.2 Fundamentals of Impedance Matching Networks.....	30
2.5.3 Argon Impedance Data	33
CHAPTER 3: METHODOLOGY	36
3.1 Modeling & Design	36

3.1.1 MATLAB Model	37
3.1.2 COMSOL Model.....	46
3.1.3 SolidWorks Model.....	49
3.1.4 Material Choices	56
3.1.5 Gas Feed In.....	58
3.2 Assembly.....	59
3.2.1 Acquisition of Materials	59
3.2.2 Fabrication of Components.....	59
3.3 Test and Facility Integration	61
3.3.1 Impedance Matching Network Design.....	63
3.3.2 Matching Network Component Selection	69
3.3.3 Facilities Integration.....	74
CHAPTER 4: CONCLUSIONS AND RECOMMENDATIONS	82
4.1 Conclusions.....	82
4.2 Recommendations for Future Work.....	87
REFERENCES.....	90
APPENDICES	92
Appendix A.....	92
0-D MATLAB Code.....	92

ABSTRACT

The goal of this project was to design and build a laboratory-model, Radio-Frequency Electrothermal thruster to operate at 300 W using a 13.56 MHz RF power supply. The thruster was designed to include an interchangeable nozzle. Two numerical models were created. The first was a 0-D global model based on an energy balance in the discharge and implemented in MATLAB. The second was a heat transfer model generated using COMSOL multiphysics software. Materials and components were selected and purchased for the thruster structure, mounting stand, gas inlet, and discharge cavity. A matching network was required to minimize reflected power in the transmission line. After a review of matching network theory, a circuit analysis was performed to design the network and select components.

LIST OF FIGURES

Figure 1. Gas Temperature vs Electron Number Density for Plasma [17]	12
Figure 2. DC Glow Discharge [19] © 1993 National Space Research Institute	13
Figure 3. Capacitively Coupled Plasma [19] © 1993 National Space Research Institute.....	13
Figure 4. Inductively Coupled Plasma [19] © 1993 National Space Research Institute	14
Figure 5. Resistojet [15]. © 2015 Wayne Schmidt.....	16
Figure 6. Arcjet [15]. © 2015 Wayne Schmidt	16
Figure 7. RFET Sample Design. [5] © 2009 by the Authors.....	18
Figure 8. “Pocket Rocket” [9] © 2009 by the Authors.....	19
Figure 9. Thrust Measurement RFET Setup [23] © 2009 by the Authors.....	20
Figure 10. Leybold Trivac D16B. © 2001, Ideal Vacuum Products	22
Figure 11 Schematic of Leybold Trivac D16B [7]. © 2001, Ideal Vacuum Products	23
Figure 12. Drawing of the Leybold Turbovac 361 [7]. © 2001, Ideal Vacuum Products	24
Figure 13. Picture of the Physical Electronics 640 I/s Ion Pump [14]. © 2014 Justin White	25
Figure 14. Schematic of T4 Vacuum System [7] © 2011 Sebastian Ryan.	26
Figure 15. Ion Density Over 2 RF Cycles [16] © 2013 by the Authors	27
Figure 16. Measurements of Optical Emission at Two Times During RF Cycle. Colors represent lines of constant optical emission intensity in reference to the global maximum. [16] © 2013 by the Authors... 28	
Figure 17. Argon Plasma Emissions [16] © 2013 by the Authors	29
Figure 18. L Matching Networks [26].....	30
Figure 19. Experimental Argon Impedance Data [28] © 1998 by the Authors	34
Figure 20. Plots for performance characteristics vs. RF power for the RFET with a throat diameter of 1mm and an expansion ratio of 50.....	42
Figure 21. Plots for performance characteristics vs. RF power for the RFET with a throat diameter of 5mm and an expansion ratio of 50.....	43
Figure 22. Plots for performance characteristics vs. RF power for the RFET with a throat diameter of 15mm and an expansion ratio of 50.....	44
Figure 23. Flow chart for the 0-D MATLAB mass and energy balance model.	45
Figure 24. Plot showing a cross section of the Quartz tube containing argon, and the temperature distribution (in Kelvin) found in each while supplied with 500W of RF power.	48
Figure 25. Preliminary design for the RFET Thruster Housings.....	50
Figure 26. Refined design for the RFET Thruster Housings.....	51
Figure 27. Final design of the RFET. Housing diameter of 5” and thickness of ½ in. Support rods are 6 in. long and quartz tube is 5 in. long.....	53
Figure 28. Bottom housing of the RFET.	54
Figure 29. Bottom Housing Cut Away with Quartz Tube and O Ring.....	55
Figure 30. Antenna Wrap on Quartz Tube.....	57
Figure 31. Swagelok Tube to Male NPT Bulkhead Fitting. [30] © 2009, Swagelok.	58
Figure 32. Aluminum Plate ready to be machined.	60
Figure 33. The final machined and assembled thruster.	61
Figure 34. Resistance vs. RF Power for Different Argon Pressures.....	64

Figure 35. Reactance vs. RF Power for Different Argon Pressures	64
Figure 36. Percentage of Power Delivered vs. Input Power (Unmatched Network)	66
Figure 37. C and L values to Match Impedance vs Input Power at 100 mTorr	67
Figure 38. Percentage of Power Delivered vs. Input Power (Matched Network)	69
Figure 39. Capacitor [33] © 2015 RF Parts Company	70
Figure 40. Inductor [35] © 2008 Coil WS	71
Figure 41. Chassis Adapters [33] © 2015 RF Parts Company	72
Figure 42. Type N Connectors [37] © 2015 Pasternack.....	73
Figure 43. Feedthrough - Property of Busek Corporation, Inc.....	76
Figure 44. Feedthrough Adapter [38] © 2014 Ideal Vacuum Systems	76
Figure 45. Picture of T4 Chamber	77
Figure 46 Flow Control and Argon Tank In Final Location	77
Figure 47 ENI OEM-650A RF Power Supply.....	78
Figure 48. NPT Fitting [30] © 2015 Swagelok	78
Figure 49. NPT Feedthrough [39] © 2015 Vacuum Research Corporation	79
Figure 50. Hose Adapter [39] © 2015 Vacuum Research Corporation	79
Figure 51. Thruster Stand CAD Model	80
Figure 52. RFET and Thruster Integration	81

LIST OF TABLES

Table 1. Boundary conditions for the COMSOL Simulation	47
Table 2. Key parameters for the COMSOL Simulation	47
Table 3. Rate of Rise Test	62
Table 4. Matching Network Components	74

ACKNOWLEDGEMENTS

The team would like to thank a number of people and organizations for their assistance in the project. Firstly, the team would like to thank NASA for loaning WPI the T4 vacuum testing chamber and the Busek Corporation for loaning the Type-N coaxial vacuum feedthrough required for the project. Also, the team would like to thank Professor Reinhold Ludwig of WPI's Electrical and Computer Engineering Department for his crucial assistance in the design of the impedance matching network. Additionally, the team would like to thank Zachary Taillefer, a PhD candidate, for his assistance with the HL016 laboratory. Zachary assisted the team in setting up the lab for the project and integrating the project into the vacuum chamber. His knowledge was extremely important and he was always willing to help. The team would also like to thank Kevin Arruda, from the manufacturing lab, and John Labrie, a senior WPI student, for their assistance in machining components for the project. Furthermore, the team would like to thank Barbara Furhman, the Mechanical Engineering Administrative Assistant, for her assistance in the purchasing of parts and maintaining the team's budget. Finally and most importantly, the team would like to thank Professor John J. Blandino, the project advisor, for all of the support, knowledge, and direction he provided in the management and completion of the project.

TABLE OF AUTHORSHIP

Section	Author
<i>ABSTRACT</i>	JB
<i>ACKNOWLEDGEMENTS</i>	ZT
<i>INTRODUCTION</i>	SO
<i>BACKGROUND</i>	
2.1, 2.2, 2.5	ZT
2.3	RB
2.4	SO
<i>METHODOLOGY</i>	
3.1.1, 3.1.2, 3.1.3, 3.1.5	RB
3.1.4	SO
3.2	RB
3.3	ZT
<i>CONCLUSIONS AND RECOMMENDATIONS</i>	
5.1	SO
<i>APPENDICES</i>	
A.1	RB

CHAPTER 1: INTRODUCTION

Radiofrequency electrothermal (RFET) thrusters are a form of electric spacecraft propulsion that uses RF power to ionize and heat a gas, accelerating it through a nozzle at high velocity to produce thrust. These kinds of thruster use inert gasses, such as xenon and argon, relying on the resulting change in pressure and temperature through the nozzle to accelerate the gas, as opposed to using either electrostatic or electromagnetic magnetic fields for acceleration.

RFET thrusters have the potential to be used applications such as orbit keeping and long duration flight of spacecraft. While they have a lower specific impulse than some other forms of electric propulsion, they can perform much better than chemical alternatives. Because an RFET thruster is essentially a cylinder containing gas heated with radiation transmitted by an antenna, followed by a simple nozzle at the far end, RFETS can be simpler in construction than other types of electric propulsion, such as Ion or Hall thrusters. In addition, RFET thrusters are still an immature technology in terms of flight heritage.

This project both designed and built a simple RFET thruster for testing in a vacuum chamber. This consisted of three main stages of the project, mathematical and conceptual design, machining and assembly, and laboratory integration. Because there are very few schematics for RFET thrusters, and none that could be found that detail all aspects of the system, extensive research and compiling of different designs had to be done to design the thruster. This lead to simplified mathematical models developed in both MATLAB (The MathWorks, Natick Massachusetts) and COMSOL Multiphysics (COMSOL, Stockholm Sweden)

For an RF current to be able to produce plasma, it was necessary to have access to a vacuum chamber capable of pumping to at least a moderate vacuum ($< 10^{-4}$ torr) [4]. To achieve this, this project was allowed use of the T4 vacuum chamber at WPI. While the chamber was capable of achieving the necessary vacuum, it was not equipped to feed in either the necessary RF power or gas flow. In order to mount the thruster in the chamber, a modular stand had to be designed to secure the thruster and protect the chamber and pumps.

In addition, work was done in developing a matching network that would ensure that a sufficient fraction of the RF power would arrive at the thruster to enable operation, instead of being reflected back into the power supply. While the power supply is capable of handling the entire reflected power, there is still a minimum amount that must reach the thruster for plasma to be created.

This project resulted in a finalized thruster design, fully assembled and started to be integrated into the T4 vacuum chamber. There remains additional work to be done to finish the facility integrations, especially regarding the matching network. It has provided the majority of the infrastructure which will be required for further testing and refinement in future years, such as alternative nozzle designs, a more efficient matching network, and use of optical spectroscopy as a diagnostic method.

CHAPTER 2: BACKGROUND

2.1 Radio Frequency Discharges

2.1.1 Plasma Basics

Plasma is the most common state of matter in the Universe. It forms when the atoms or molecules of a gas are ionized, resulting in a mix of charged and neutral particles that behave as an electrically conducting medium. It is often useful to characterize a plasma with respect to whether the electrons are in thermal equilibrium with the heavy species, i.e. ions and neutral atoms. In such situations, a plasma can be broken down into two main categories; thermal and non-thermal. In thermal plasmas, partial or full ionization takes place due to heating of the neutral gas, which then exchanges energy with electrons, atoms and molecules through collisions. If the neutral gas is sufficiently energetic, then collisions with neutral atoms can result in ionization, which produces additional ions and electrons. The high rate of collisions result in the plasma being in thermal equilibrium. Thermal plasmas typically require temperatures ranging from 4,000 to 20,000 Kelvin in order for a sufficient amount of gas molecules to be ionized [16]. In non-thermal (or non-equilibrium) plasmas, the electrons are typically at a much higher temperature than the heavy species. By applying an electric or magnetic field to the gas, electrons can be accelerated (i.e. heated”) to high energy without greatly increasing the temperature of the (more massive) ions and neutral gas atoms. Non-thermal plasmas are often referred to as “cold” plasmas. The degree of ionization of non-thermal plasmas is typically lower than that of thermal plasmas. This can be seen in Figure 1 below which shows the density of electrons (and thus ionization density) versus the gas temperature.

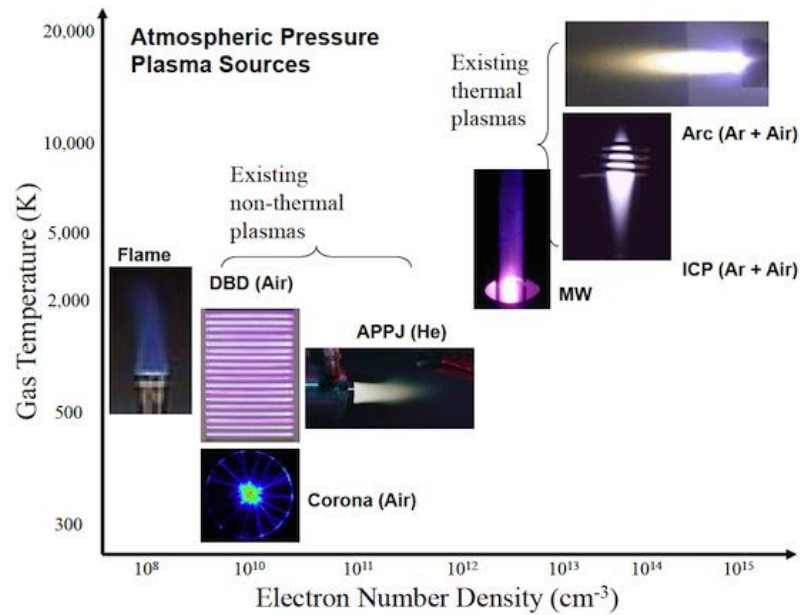


Figure 1. Gas Temperature vs Electron Number Density for Plasma [17]
© 2014 Yongho Kim

Both types of plasmas occur widely in industry, in processes such as plasma cutting torches (thermal) and plasma assisted deposition (thermal or non-thermal) [2,10,12]

2.1.2 Plasma Generation

Plasmas in which electric fields are used to add energy to electrons can be broken down into two categories: direct-current, glow discharges and radio frequency (RF) discharges. Direct-current (DC) glow discharges are generated by applying a DC voltage in order to create an electric field in the gas (Figure 2) and RF discharges result when a (alternating current), RF electric field is coupled to the electrons in the gas. The most common frequency used to produce RF discharges is 13.56MHz because it is commonly used for industrial, scientific and medical applications [17]. The electric field can either be coupled capacitively or inductively to the discharge. In capacitively coupled plasmas (CCP), the gas atoms are ionized by two

electrodes placed inside the discharge chamber (Figure 3). Inductively coupled plasmas (ICP) result from energy provided by electromagnetic induction (Figure 4). The electrical energy can either be transferred from a coil placed at one end of the discharge chamber, or from a helical shape coiled around the discharge chamber. A major advantage of ICPs is that the electrodes are located outside of the discharge chamber, which avoids the erosion due to “sputtering,” sometimes seen in CCPs, in which the electrodes are located inside the discharge chamber. Magnetic fields can also be used in tandem with RF discharges in order to control or manipulate the plasma. This project focuses on generating a radio-frequency, inductively coupled plasma for use in an electrothermal thruster, a type of electric propulsion [13].

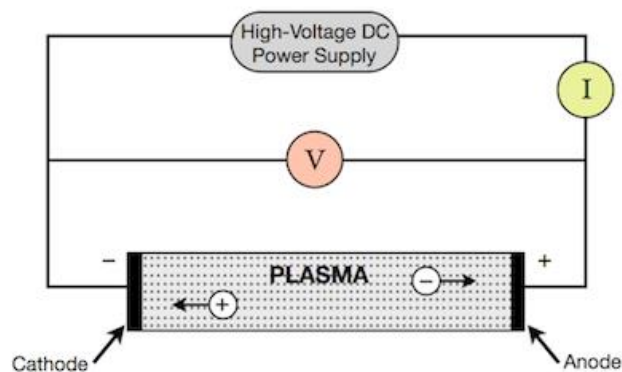


Figure 2. DC Glow Discharge [19] © 1993 National Space Research Institute

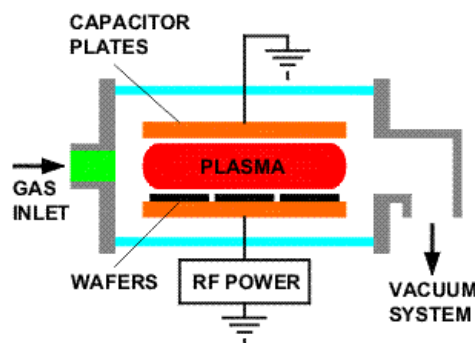


Figure 3. Capacitively Coupled Plasma [19] © 1993 National Space Research Institute

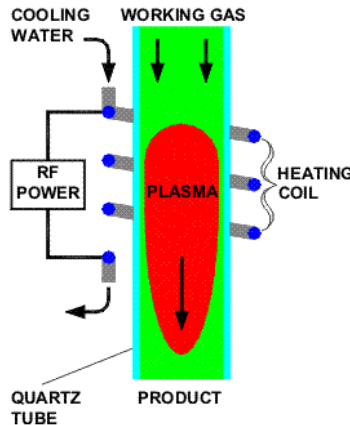


Figure 4. Inductively Coupled Plasma [19] © 1993 National Space Research Institute

2.1.3 E and H Mode

Inductively coupled discharges can occur in one of two “modes” called the E and H modes. The E mode is seen at low power to mass flow ratios as soon as the plasma discharge forms and is known as the capacitive mode. The E mode discharge is sustained by the generated electrostatic field. At higher power inputs, a transition to H mode takes place. The H mode is also known as the inductive mode and yields greatly increased chamber temperature and pressure due to a more efficient transfer of energy from the power source to the gas molecules [18]. E mode consists of a low electron density, low light emission, and high electron temperature. H mode, with increased input power, results in a much higher electron density, a marginally lower electron temperature, and greatly increased light emission. The transition from E to H mode occurs suddenly with increased input power [12]. The gas flow rate and chamber pressure will affect where this transition takes place. However, the transition from H to E mode occurs at a lower input power than the E to H mode transition. This occurrence is known as hysteresis and is valuable for plasma generation because the power can be lowered

once H mode is initiated. So a spike in power is all that is needed to make the transition to H mode, then the power can be reduced to save energy [11,12]

2.2 Radio Frequency Electrothermal Thrusters (RFET)

2.2.1 Principles of Operation

Electric propulsion systems utilize electrical energy in order to generate thrust by expelling partially ionized, propellant gas at a high speed. There are three main types of electric propulsion systems: electrostatic, electromagnetic, and electrothermal thrusters. The systems are differentiated by the method by which they accelerate the gas to produce thrust.

Electrostatic thrusters accelerate ions using high voltage electrodes to create strong electric fields which then accelerate the particles via the Coulomb force. Electromagnetic thrusters make use of magnetic and electric fields to accelerate ions using the Lorentz ($\mathbf{j} \times \mathbf{B}$) force.

Lastly, electrothermal thrusters use electric power to heat a gas, and then use a conventional nozzle accelerate the propellant gas to high speed [19].

This project specifically focuses on one type of electrothermal thruster. Various types of electrothermal thrusters exist, such as resistojets and arcjets. Resistojets heat the propellant gas via a resistor located in the discharge chamber, while arcjets transfer energy to the gas through an electric arc, with current flowing between a cathode and anode located in the discharge chamber [19]. Figures 5 and 6 below show a resistojet and an arcjet, respectively. Other types of electrothermal thrusters exist in which the energy is inductively-coupled. These are typically only identified by the frequency band of their power source. Two commonly used frequency bands include microwave, from between 300MHz and 300GHz [15], and radio-

frequency, ranging from 3 kHz to 300GHz. This project involves a radio frequency electrothermal thruster (or RFET) operating at 13.56 MHz.

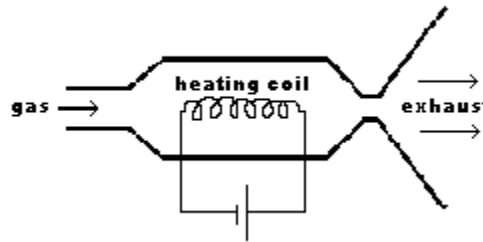


Figure 5. Resistojet [15]. © 2015 Wayne Schmidt

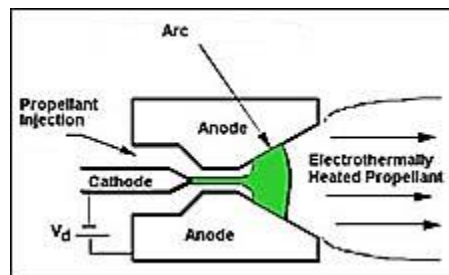


Figure 6. Arcjet [15]. © 2015 Wayne Schmidt

A radio frequency electrothermal thruster typically involves a tube for a discharge chamber, an antenna or coil, and a nozzle to accelerate the expelled the gas. The antenna delivers the power from a radio frequency (RF) power source to the discharge chamber via magnet wire or a water-cooled copper tube coiled around the chamber [32]. The power coupled to the electrons in the tube accelerate them, so they in turn collide with and ionize gas molecules. This, in turn generates a plasma in the discharge chamber, with greatly increased temperature. The discharge chamber consists of a cylindrical quartz or Pyrex tube, due to their low loss dielectric properties [21]. The gas injector is located at one end and the nozzle at the other end of the chamber tube. The nozzle serves to accelerate the excited propellant and can

range in complexity. Some RFETs do not use a nozzle at all. Other versions take advantage of magnetic forces in combination with electrostatic forces to further increase the velocity of the exiting gas (Helicon thrusters)[20]. Gases with low molecular weights are mostly preferred for research version of these thrusters, with helium (He) and argon (Ar) being the most common among them.

There are a couple advantages to the RFET design over other electrothermal thrusters. Firstly, the design is simple to manufacture as it consists of just a tube, wire antenna, a power source, nozzle, and basic housing components. Another advantage over resistojets and arcjet designs is that the antenna in a RFET does not contact the propellant but instead delivers power through the chamber tube. This minimizes the electrode erosion associated with a discharge such as an arcjet.

2.2.2 Pennsylvania State University RFET

For this project, the most relevant previous work found to serve as a starting point was a low power (100W) RFET designed at Pennsylvania State University [5]. Their design can be seen below in Figure 7. The experiment used a quartz tube as a discharge chamber with two aluminum housings on either end, both sealed with O-rings. The diameter of the quartz tube was unknown. On one end of the chamber was a stainless steel nozzle plate with a convergent-divergent exhaust nozzle with an unknown expansion ratio. To provide the power, a 100 Watt source was used along with an Ameritron AL-1200 RF amplifier to increase power output. The amplifier was needed to initiate H-mode plasma, where around 140 W was required. The power source was connected to 18 AWG magnet wire wrapped around the quartz tube roughly

14 times. The propellant gas (Helium) was introduced into the discharge chamber via a tangential injector with mass flow rates ranging from 0.43 mg/s to 1.08 mg/s.

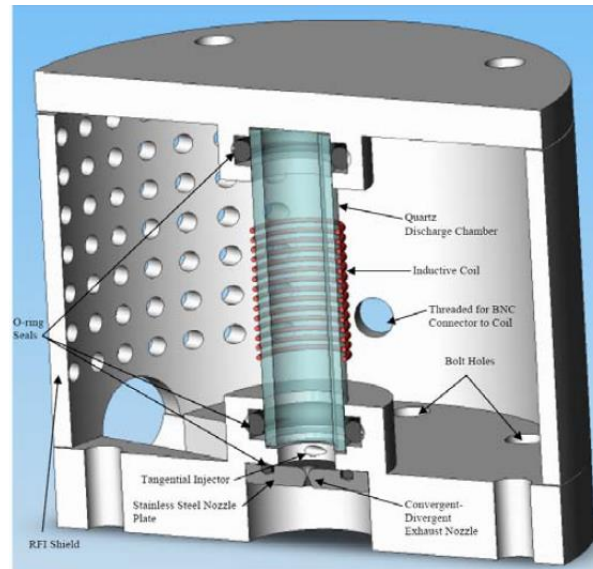


Figure 7. RFET Sample Design. [5] © 2009 by the Authors

The experiments conducted by the Penn State team were mostly focused the transition from E mode to H mode. They studied how much power was required to make this transition in the plasma and whether or not H mode could be sustained at lower power than required to initiate the transition from E mode. They concluded that it was possible when the thruster transitioned from E mode to H mode at 140 Watts of power and then were able to reduce the power to 100 Watts and still maintain H mode [5].

This project was particularly useful to our own because relatively few papers exist on the topic of RFET propulsion. The information provided in the paper gave us the most insight into designing our own RFET out of the papers reviewed.

2.2.3 Pocket Rocket RFET

A second experiment that provided guidance in the design for this project was a joint effort between C. Charles, R.W. Boswell and J. Dedrick from the Australian National University and D. O’Connell and T. Gans from the York Plasma Institute in the United Kingdom [9]. This paper was focused primarily on the optical spectroscopy of a RFET plume, but still provided information used in sizing the thruster for this project. Their designs were nicknamed a “pocket rocket” due to its very small size and input power. This thruster used a 12.50 MHz RF power source. The discharge chamber tube was only 2 cm long and 4.2 mm in diameter. Argon gas was used as propellant at a pressure of 1.5 torr. Their estimated discharge chamber pressure was 1 torr. This paper provided background information for the sizing and scaling of RFET thrusters. The “pocket rocket” can be seen in the image below [9]. More information and further studies of this micro-thruster design can be found in another paper by The Australian National University where the neutral gas heating of the “pocket rocket” was analyzed [3].

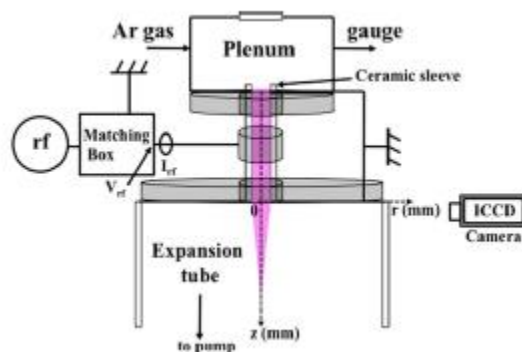


Figure 8. “Pocket Rocket” [9] © 2009 by the Authors

2.2.4 Variable Length RFET

This paper, also from The Australian National University partnered with Iwate University in Japan, provides another source of information used in sizing the thruster for this project [23]. It focuses on thrust measurements using a pendulum thrust balance and laser displacement sensor. They obtained about 2 mN of thrust at 700 W of input power using a discharge chamber length of 17.5 cm and a mass flow rate of 0.9 mg/s of argon. They also tested a shorter discharge chamber with a length of 9.5 cm. This shorter version produced 4 mN of thrust at a similar power and a flow rate of 1.65 mg/s. The RF power source used for these experiments operated at 13.56 MHz. A Pyrex tube was used in both setups with a diameter of 6.4 cm and a copper double-turn loop antenna. The paper also mentions that a type of impedance matching network, called a Pi network, was used in the experimental setup [23]. A schematic of the setup is seen below.

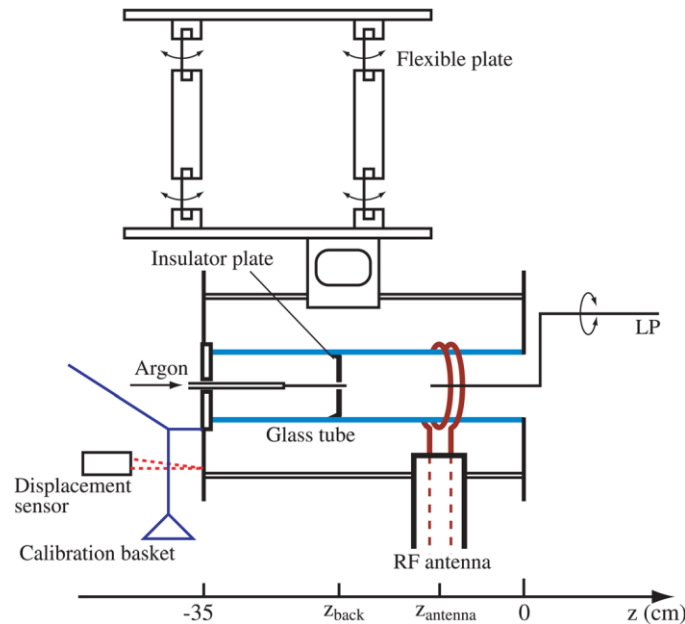


Figure 9. Thrust Measurement RFET Setup [23] © 2009 by the Authors

2.3 Vacuum System Technology

2.3.1 Need for a Vacuum

The intended application of this thruster, as previously stated, is for propulsion on spacecraft in deep space flight, or the repositioning of satellites currently in orbit. In both of these cases, the thruster will fire at essentially vacuum conditions. It is estimated the exit pressure at the nozzle's exit will be anywhere from 0.001 to 0.2 atm. Because a rocket's thrust is a function of the difference between the pressure at the nozzle's exit and the back (or ambient) pressure, it is evident that to adequately simulate and test the thruster's performance and efficiency, it is vital that the thruster operate within a vacuum chamber.

Additionally, a mass flow rate will be introduced to the vacuum during the thruster's operation. Therefore, in order to maintain a constant back pressure in the chamber, the vacuum pumps must be able to remove the gas at or near the same rate it is being introduced. As the gas, which has been chosen to be argon, is expelled, it cannot be directly introduced in the surrounding air, and must be vented to another source to maintain the quality of the air within the lab. Argon was chosen to be the gas for testing because of its accessibility and the abundance of data on argon plasma discharges. The other possible gas for testing was xenon, but it was ruled out because of cost.

All tests will be performed in the WPI Vacuum Test Facility's (VTF) Tank 4 (T4). The tank's vacuum system is described in the following sections.

2.3.2 Vacuum Pumps

Three separate pumps will be used during experiments for this project to adequately establish and maintain a vacuum in which the thruster can operate. In order for the desired back pressure to be achieved within the chamber, these pumps will operate in succession. The first of these pumps is the Leybold Trivac D16B, a rotary-vane dual-stage mechanical pump shown in Figure 10.

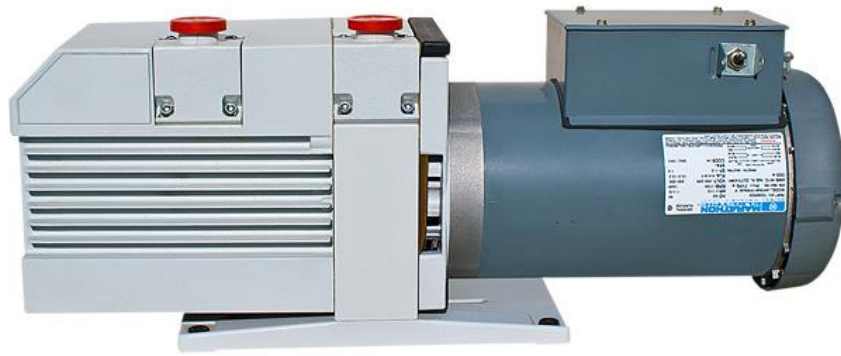


Figure 10. Leybold Trivac D16B. © 2001, Ideal Vacuum Products

It produces a vacuum using two off-center rotors, which are attached to spring loaded vanes and share a shaft. Leaks are prevented by maintaining a seal between mechanical components with a thin layer of lubricating oil. Gas enters the system and is compressed in a volume by one of the rotors, it is then exhausted to the second rotor and compressed further. The compressed gas then passes through a one-way valve into the next vacuum pump. A schematic of the D16B is shown in Figure 11.

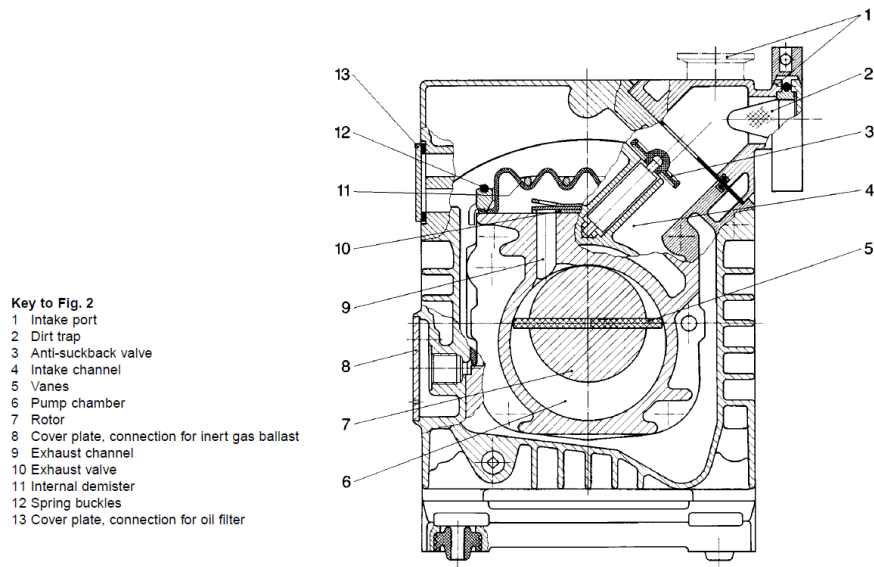


Fig. 2 Sectional drawing of the TRI/VAC-B

Figure 11 Schematic of Leybold Trivac D16B [7]. © 2001, Ideal Vacuum Products

The rotary pump serves as a roughing pump, or the backing pump for the turbomolecular pump, the Leybold Turbovac 361. This second pump will be turned on once the roughing pump attains a chamber pressure of 0.1 Torr. The Leybold Turbovac 361 is shown in Figure 12 below.

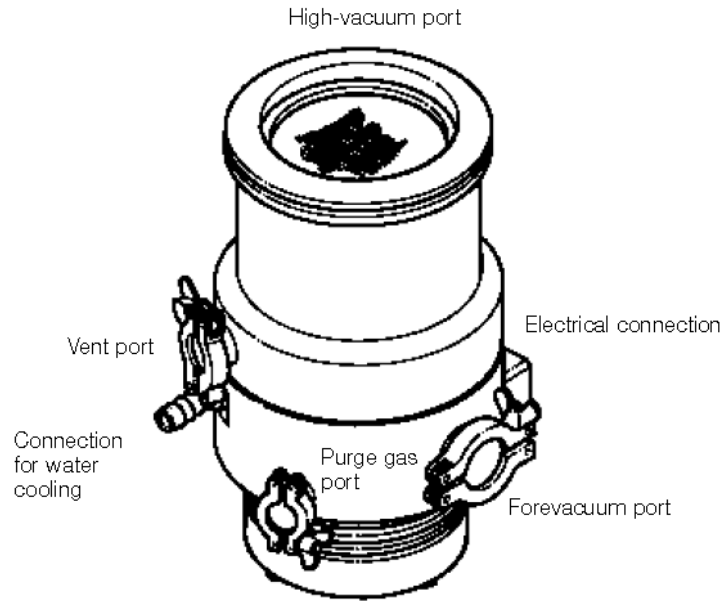


Figure 12. Drawing of the Leybold Turbovac 361 [7]. © 2001, Ideal Vacuum Products

The turbomolecular pump operates on the same general principal as the rotary pump, but uses a turbine spinning at a much higher rpm. The turbine's blade tips move at close to mean speed of the gas molecules, which allow it to operate in the molecular flow regime and further decrease the amount of gas present within the vacuum chamber, thus improving the vacuum. The pump is usually run in series with another pump, often a rotary pump such as the D16B, due to the fact that the compression ratio of the system approaches an order of magnitude when the incoming gas is at 0.1 Torr. The compression ratio drops, however, to 10 when the incoming gas pressure increases to 1 Torr.

If vibration due to the turbomolecular pump were an issue, the third and final pump could be used once the pressure is sufficiently low. This is the Physical Electronics 640 I/s Ion Pump, which is pictured in Figure 13. Vibration is not of concern for the RFET tests and there was no need to use the ion pump.



Figure 13. Picture of the Physical Electronics 640 I/s Ion Pump [14]. © 2014 Justin White

As with the turbomolecular pump, the ion Pump would only be activated once a certain pressure is attained within the vacuum, in this case if the pressure is below 1 mTorr. In this pump, a magnetically confined electrical discharge is established between an anode and a cathode, both made out of highly conductive metals. The discharge ionizes the molecules being introduced to the system. The ions are then attracted to the cathode by the electric field where they impact and sputter the surface, forming metallic compounds which are trapped as a coating on the anode surface.

2.3.3 Vacuum Measurements

There are three gauges in the system which will measure pressure. These are each shown in Figure 14.

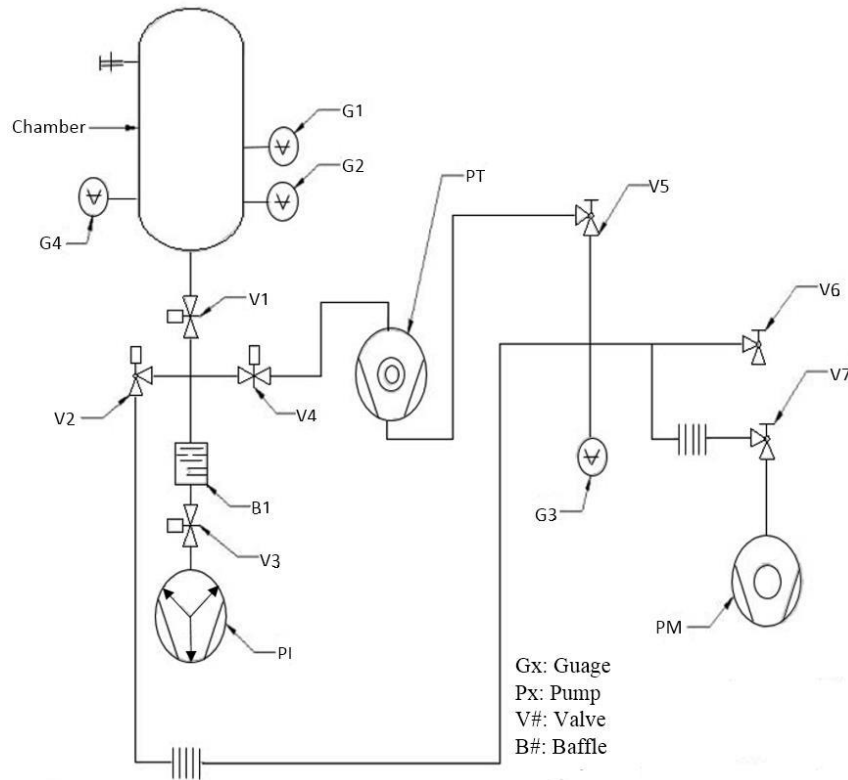


Figure 14. Schematic of T4 Vacuum System [7] © 2011 Sebastian Ryan.

The first two gauges, G1 and G2, are both Leybold Thermovac T221 thermocouple gauges. They measure the thermal conductivity of the gases present, which can then be correlated with the chamber pressure. The third gauge, G4, is a Varian Agilent model 572 Ionization gauge. G4 will only be used if the vacuum chamber is operating at pressures below 1 milliTorr, as the filament used to ionize the gas would erode and fail at pressures above this value.

2.4 Optical Spectroscopy

2.4.1 General Principles

Optical Spectroscopy is the study of the properties of physical objects based on the absorption and emission of light. It is primarily used to measure characteristics such as an

object's chemical composition, temperature and velocity. Optical spectrometers are used to study a medium's ability to alter propagation velocity and amplitude of light. This is a form of emissions spectroscopy, where the medium is excited with the use of an outside energy source (light or heat) causing excited particles to emit light (photons) as they transition to lower energy levels. The energy released and wavelength of the photons differs for different gases, which is measured and analyzed. Optical spectroscopy is often used to determine the composition and density of a particular discharge. While determination of quantitative information such as ion density involves the use of sophisticated radiation models, qualitative information on the shape of the excited region and identification of specific excited states, are easier to obtain.

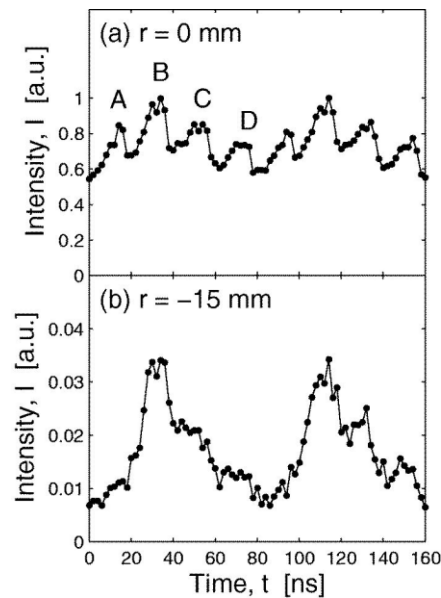


Figure 15. Ion Density Over 2 RF Cycles [16] © 2013 by the Authors

2.4.2 Previous Spectroscopic Studies of RFET Thrusters

Optical Spectroscopy has been used previously on radio frequency electrothermal thrusters. The technique was used to analyze the shape and intensity of a discharge plume of a

“Pocket Rocket” micro thruster over the course of an RF cycle [13]. The “Pocket Rocket” is a micro RF thruster measuring 4.2mm in diameter and uses power ranging from 1 to 100 watts at a frequency of 13.56 MHz. Analyses showed four peaks of emission intensity during an RF cycle, meaning that the coil antenna was causing the gas to ionize at twice the rate expected from simple RF sheath heating as shown in Figure 15. In addition, the plume shape and intensity was observed at different times and power levels. In the “Pocket Rocket”, without a nozzle, the maximum plume length and diameter was achieved at the lowest pressure (see Figure 16). The plume diameter measured about twice the diameter of exit cavity. It is evident from Figure 16 that throughout the course of an RF cycle, the shape of the plume changes, increasing in diameter greatly, but experiences little change in length.

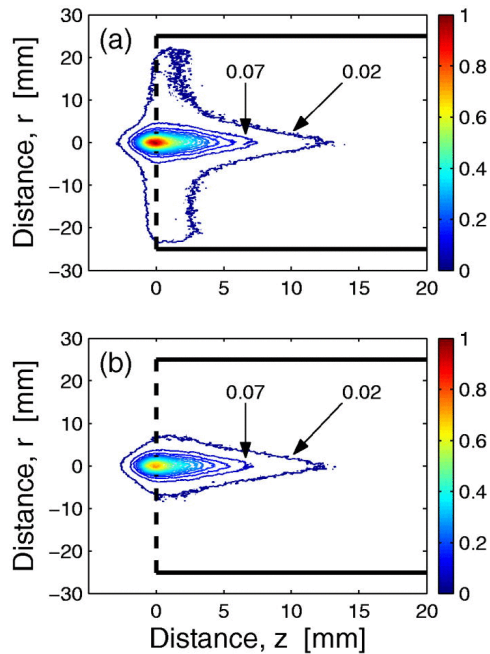


Figure 16. Measurements of Optical Emission at Two Times During RF Cycle. Colors represent lines of constant optical emission intensity in reference to the global maximum.
[16] © 2013 by the Authors

2.4.3 Visual Characteristics of Argon

The spectrometer will be used by future groups to verify the expected optical emissions of the plume and identify any unexpected ions. Figure 17 shows the expected spectra for nearly pure argon plasma. The majority of wavelength spikes are between 700 and 800 nm with lower intensity peaks around 550 and 650 nm. The presence of other elements, such as oxygen, which may be present as residual gas in the vacuum chamber, and will be evident by peaks at different wavelengths.

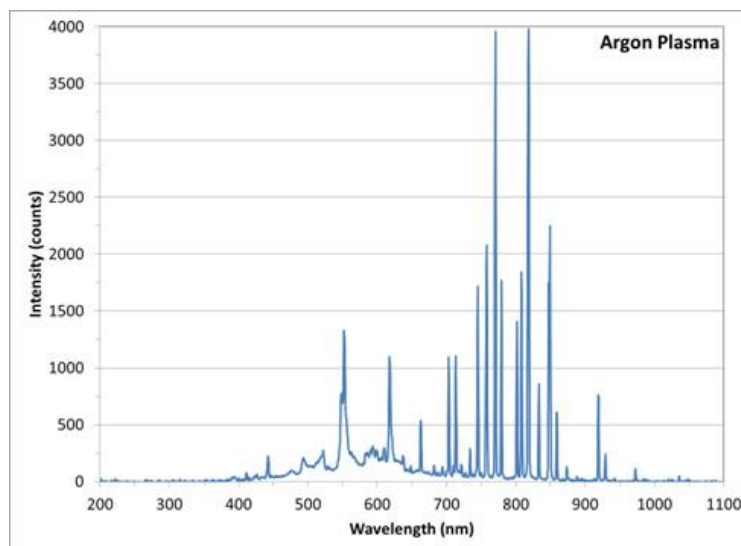


Figure 17. Argon Plasma Emissions [16] © 2013 by the Authors

2.5 Impedance Matching Networks

2.5.1 Importance of Impedance Matching Networks

Impedance matching is essential in the transmission of radio-frequency (RF) power. Impedance is the combination of resistance and reactance that occurs from alternating currents. Resistance is the only form of impedance that occurs in DC circuits. In alternating currents, such as RF, an “imaginary” part of the impedance must be included. This is the

reactance. The goal of impedance matching is to match the impedance of the source to the impedance of the load so that all of the power can be delivered to the creation of plasma. Without a matching network, a large percentage of power can be reflected backward toward the RF power source. Depending on the power source, this could potentially damage it. Impedance matching is necessary to minimize the reflected power and therefore effectively transmit RF power to the load. For the RF thruster, the load is the plasma discharge, which is heating the gas before it is expelled and accelerated through the nozzle.

2.5.2 Fundamentals of Impedance Matching Networks

Impedance matching networks can take many forms, both simple and complex. There are three primary types of matching networks: L, Pi, and T networks [24]. L-Networks are the simplest and consist of only two components, a capacitor and an inductor. It gets its name because it looks like a sideways “L” in the circuit design. This network rather simply equalizes the impedance of the source, Z_0 , and the impedance of the load, Z_L . The inductor and capacitor can be arranged in a number of ways depending on the desired match, but the two most common are show below in Figure 18.

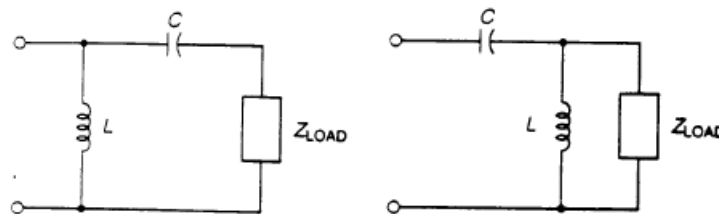


Figure 18. L Matching Networks [26]

The design on the left would be used when the source impedance is greater than the impedance of the load ($Z_s > Z_L$). The inductor, L , is placed in parallel with the source and the capacitor is placed in series with the load in order to negate the reactance. The design on the right is used when the impedance of the source is less than the impedance of the load ($Z_s < Z_L$). Here, the inductor, L , is placed in parallel with the load and the capacitor is placed in series with the source to negate the reactance.

The load impedance of a discharge generating plasma is typically higher than the source impedance, as discussed in section 2.5.3. Because of this, the design on the right is relevant to this project. In order to size the necessary capacitor and inductor, the source and load resistance, R_s and R_L , must be known. The frequency of the RF power source must also be known. These resistances are then used to calculate the quality factor, Q . The quality factor represents a ratio between the inductance and resistance and is useful in examining the efficiency in RF circuits. This can be obtained by using equation 1. The quality factor is unitless [26].

$$Q = \sqrt{\frac{R_L}{R_s} - 1} \quad (1)$$

With a known quality factor, the reactance of the load and source, X_L and X_s , can be calculated by Equations 2 and 3. These quantities are measured in ohms, but represent the imaginary portion of the impedance.

$$X_s = QR_s \quad (2)$$

$$X_L = \frac{Q}{R_L} \quad (3)$$

After obtaining the reactance of the load and source, the C and L values for the capacitor and inductor can be calculated by from these values and the frequency of the RF power source. Equations 4 and 5 are used to calculate C and L [26]. C is measured in farads and L is measured in henries.

$$C = \frac{1}{2\pi f X_L} \quad (4)$$

$$L = \frac{X_s}{2\pi f} \quad (5)$$

These values for C and L are those required to match the impedance of the source and load. In many cases with plasma discharges, the impedance of the load will change with time as operating conditions change. The impedance of the load can change with the power input, gas density in the chamber and the state of the plasma, including whether or not plasma has ignited yet. In order to help address this, a variable capacitor can be used. Variable inductors are available but the range of inductance is minimal. Therefore, variable capacitors are typically used with fixed inductors. The capacitors can be tuned to match a wide range of load impedance. This setup is used in reference [27].

The other types of networks, Pi and T, give some benefits over the L matching networks [24]. Pi networks are essentially two L networks together. The major benefit of a Pi network is that, with the increased amount of components, the designer can set the quality factor for the circuit. This is beneficial in matching amplifier outputs. T matching networks are useful when matching to relatively low impedance and with a low quality factor value. These are used for

both transmission line impedance matching and solid state amplifier designs [24]. Because the impedance of a plasma discharge is higher than the source impedance and the quality factor does not matter, T and Pi networks should not be needed for this work. L impedance matching networks are the most practical for plasma discharge purposes.

Another important factor in RF circuits is the length of the cable that runs from the power supply to the matching network itself. RF waves have a wavelength, λ , that is a function of the wave speed, frequency, and “velocity factor” of the specific cable. The velocity factor is a unitless parameter that describes how quickly the waves travel through the cable. The length of cable running from the source to the matching network should be a quarter of the total wavelength for proper matching [25]. If this is not the case, the waves will reflect backward and decrease transmission of power. So, in order for the impedance matching network to work properly, the cable length must be a quarter-length of the wavelength. The wavelength can be calculated by Equation 6, where C represents the speed of light and f represents the frequency of the signal.

$$\lambda = \frac{C}{f} * Velocity Factor \quad (6)$$

The velocity factor ranges from 0 to 1 and are commonly found in the technical specifications for coaxial cables used in RF transmission [25].

2.5.3 Argon Impedance Data

The most significant difficulty in building an impedance matching network for a RFET thruster is the unknown load impedance. Without knowing a baseline range, it is very difficult to size the inductor and capacitor for impedance matching. Reference [28] is very helpful in

this regard and provides experimental impedance values for argon gas in a cylindrical discharge chamber with a wire antenna. A graphite cylinder with a diameter of 4.5 cm and a length of 6 cm was used, surrounded by a 6-turn antenna coil [28]. The layout of the experiment that yielded this data is very similar to designs typically used in RFET thrusters. It uses a 13.56 MHz RF power source with power ranging from 500 to 5,000 watts. The data is split into two plots, with one representing the resistance vs RF power and the other displaying (imaginary) reactance vs RF power. Each plot presents the data at three pressures: 10, 100 and 1000 mTorr. These plots can be seen below in Figure 19.

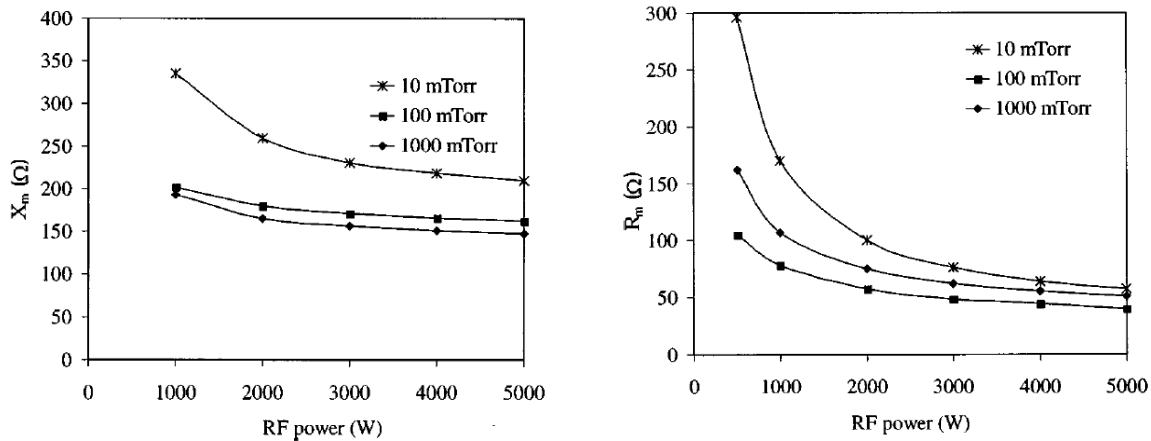


Figure 19. Experimental Argon Impedance Data [28] © 1998 by the Authors

This data is helpful as a starting point for sizing an impedance matching network for a Radio-frequency Electrothermal Thruster. This data allows calculations to be made for the capacitance and inductance required to match the impedance. However, it also gives insights into the trends corresponding to changes in pressure. When using a variable capacitor in a

matching network, this data allows for calculating what capacitance is required to “tune” the circuit.

CHAPTER 3: METHODOLOGY

3.1 Modeling & Design

The design of the RFET began with a study of similar thrusters, to develop an idea of the dimensioning to be used on the RFET. All of the dimensions are ultimately driven by the size of the discharge chamber. This was sized based on two main factors, previous RFET thruster of a similar power and commonly available sizes of quartz tubing. Other thrusters had a quartz tube ranging in diameter from about 3 mm at 10 watts and 0.43 mg/s gas flow rate [9] to 6.2 cm at 500 watts and 1.65 mg/s gas flow rate [4]. Based on the expected power output and gas flow rate (300 Watts, 0.75 mg/s) an internal diameter of 25 to 30mm was chosen. Based on the price of different combinations of internal and external diameters around 30mm, a final tube size of ID 30mm and OD 33mm was chosen, corresponding to a wall thickness of 1.5 mm. Although a tube with a slightly thicker wall would have been preferable, the significant increase in cost made it unreasonable. The length of the tubing was chosen to be 5 inches, because of the cost of cutting longer tubes to custom sizes.

Once proper dimensions for the quartz housing were determined, a series of mathematical models and simulations were developed using MATLAB and COMSOL. Hand calculations were used to check the computer code for errors. The gas chosen for testing was argon, because of its low cost and safety. The use of an atomic species also simplifies the necessary equations. The first model developed was a MATLAB script to estimate performance based on isentropic flow through the nozzle, with chamber conditions based on a particular set of parameters.

3.1.1 MATLAB Model

Initially, the model was developed to take into account some of the more advanced plasma physics, resulting in for the need to define argon's various plasma parameters, such as its Bohm Velocity, etc. However, these calculations were deemed unnecessary, as modeling simulations for these parameters would be too time consuming. Therefore, the model was simplified to consist of a global, 0-D energy and mass balance, with added heat provided by the RF Antenna, to estimate the chamber temperature and pressure. This could then be used to calculate performance assuming isentropic flow through the nozzle. This also took into account the changes the argon's ionization fraction. The MATLAB code iterated for an estimated value of the heavy particle (argon atoms and ions) temperature T_0 . This value was then used in the isentropic flow calculations in Eq. (7) and Eq. (8)

$$T'_0 = \frac{\dot{Q}}{\dot{m}C'_p} + T_{in} \quad (7)$$

$$P'_0 = \frac{\dot{m}}{\gamma A_t} \sqrt{\frac{1}{\gamma R T'_0} \left(\frac{2}{\gamma + 1} \right)^{\frac{\gamma+1}{\gamma-1}}} \quad (8)$$

First, the initial estimate of the temperature T'_0 estimated using eq. (7), where \dot{Q} is the RF power delivered to the system in Watts, \dot{m} is the mass flow rate through the chamber in kg/s, C'_p is the heat capacity of the argon gas, and T_{in} is the inlet temperature of the gas, assumed to be 273K. The value of T'_0 was then used in the isentropic equation calculating for stagnation pressure, with γ being the ratio of specific heats for argon, A_t the area of the nozzle's throat, and R the gas constant for Argon. The composition (i.e. mole fraction) X_i of the argon plasma was then calculated, yielding a new specific heat C'_p , and allowing recalculation of T'_0 . If the newly calculated T'_0 converged to a particular value, within a tolerance of less than

0.01, then the newly calculated T'_0 was used for the performance calculation. If convergence was not achieved, then the calculated T'_0 was used as the new guess, and the process was repeated.

This system of equations proved to be too rudimentary, and yielded temperature to the 9th order of magnitude Kelvin. The astronomically high temperatures were because no heat losses were accounted for as part of the model's calculation. Therefore, the next version of the model involved the heat losses associated with the ionization of argon within the thruster chamber. The script written can be found in Appendix A.

The new model also included an interface asking the user to enter an expansion ratio for the nozzle of the thruster. This expansion ratio was then used in the isentropic calculations for the temperature and pressure within the discharge chamber. The program looked through an isentropic flow table for the stipulated expansion ratio, then generated values for the ratios of static temperature and pressure to their corresponding stagnation values. Because the flow was assumed to be isentropic, the pressure and temperature within the quartz tube was assumed to correspond to the calculated stagnation values.

Calculation in the new model began much like the first, where a value for T'_0 was calculated using Eq. (7), and a corresponding value for P'_0 was then calculated, using the same isentropic flow equation Eq. (8). However, where this model differs, is in its calculation of the composition of the argon plasma within the chamber. The original model treated the separation of electrons from argon atoms as a simple reversible dissociation reaction, where the molar fractions of argon ions, and electrons were calculated and served as the degree of

ionization at a given temperature. However, this technique was very inaccurate, as it did not take into account the heat losses present in the actual ionization of the argon gas, and therefore yielded unrealistically high values for temperature. The degree of ionization was then calculated using the Saha equation, which is shown below [15].

$$\alpha \approx Gp^{-\frac{1}{2}}T^{\frac{5}{4}}e^{-\left(\frac{\varepsilon_i}{2kT}\right)} \quad (9)$$

The equation solves for the degree of ionization, α , using the guessed values of T'_0 and P'_0 for T and p , and G being a constant for argon independent of T . ε_i and k are the first ionization energy of argon in Joules, and the Boltzmann constant, respectively. Next, the initial number of moles of argon was defined to be n_0 . From the resulting value of α , the mole fractions for argon atoms, electrons, and argon ions can then be easily calculated as shown in Eq. (10) and Eq. (11). These molar values could then be used to calculate the temperature of the argon plasma using energy balance given a specific RF power input (\dot{Q}), molar flow rate of argon (\dot{n}_{AR0}), constant enthalpy of formation (\bar{h}_f°), and specific heat (\dot{n}_{AR0}). The equation relating these, solved from the energy balance equation for a mixture, is shown below in Eq. (12).

$$n_{AR^+} = n_e = n_0\alpha \quad (10)$$

$$n_{AR} = n_0(1 - \alpha) \quad (11)$$

$$T = \frac{\left(\frac{\dot{Q}}{\dot{n}_{AR0}}\right) - n_{AR^+}\bar{h}_f^\circ}{c_p(n_e + n_{AR} + n_{AR^+})} \quad (12)$$

Because the electrons present are only those produced as a result of ionization of argon atoms, the number density of electrons n_e will be equal to the number of argon atoms n_{AR^+} .

Thus, the remaining argon atoms, which were unionized, n_{AR} , will be one minus the degree of ionization. However, with the only energy sink being the ionization energy loss, the calculation still yielded unrealistically high temperature values in the chamber, therefore underscoring the need to include further heat losses, in this case those due to radiation. The equation for radiation energy loss is shown in Eq. (13) below, where P is net radiated power, ϵ is emissivity, σ is Stefan's constant, A is the radiating area, and T is the temperature of radiator [22]. Subtracting the power lost due to radiation from the power exhibited by the RF antenna provides a much more accurate value for the heat contained within the chamber and used for heat the argon

$$P = \epsilon \sigma A T^4 \quad (13)$$

After conducting a literature review of heat radiation, the emissivity for argon plasma in a cylindrical discharge was found to be 0.001 [40]. This value is for cylindrically stored plasma, and was determined by analyzing a plot in the referenced text comparing this value at different pressures. The calculated power found from the guessed T value was then incorporated into the combined heat loss and Saha equation to find the actual temperature. The new energy balance equation is shown below, incorporating the power lost through radiation.

$$T = \frac{\left(\frac{\dot{Q} - P}{n_{AR0}} \right) - n_{AR} \bar{h}_f}{c_p (n_e + n_{AR} + n_{AR+})} \quad (14)$$

The same iteration technique used in the first version of the mathematical model was then used in this instance as well, where the initial guess of temperature was compared to that resulting from the equation above, if the difference between the two fell below a specified tolerance, equal to 0.0001, the temperature was used. If not, the calculated value of T was

placed back into the iteration as the guess. The plots for temperature, pressure, specific impulse, and thrust at a set expansion ratio of 50 are shown in Figures 20, 21, 22, with varying mass flow rates and throat areas. A flow chart for the mathematical model is shown in Figure 23.

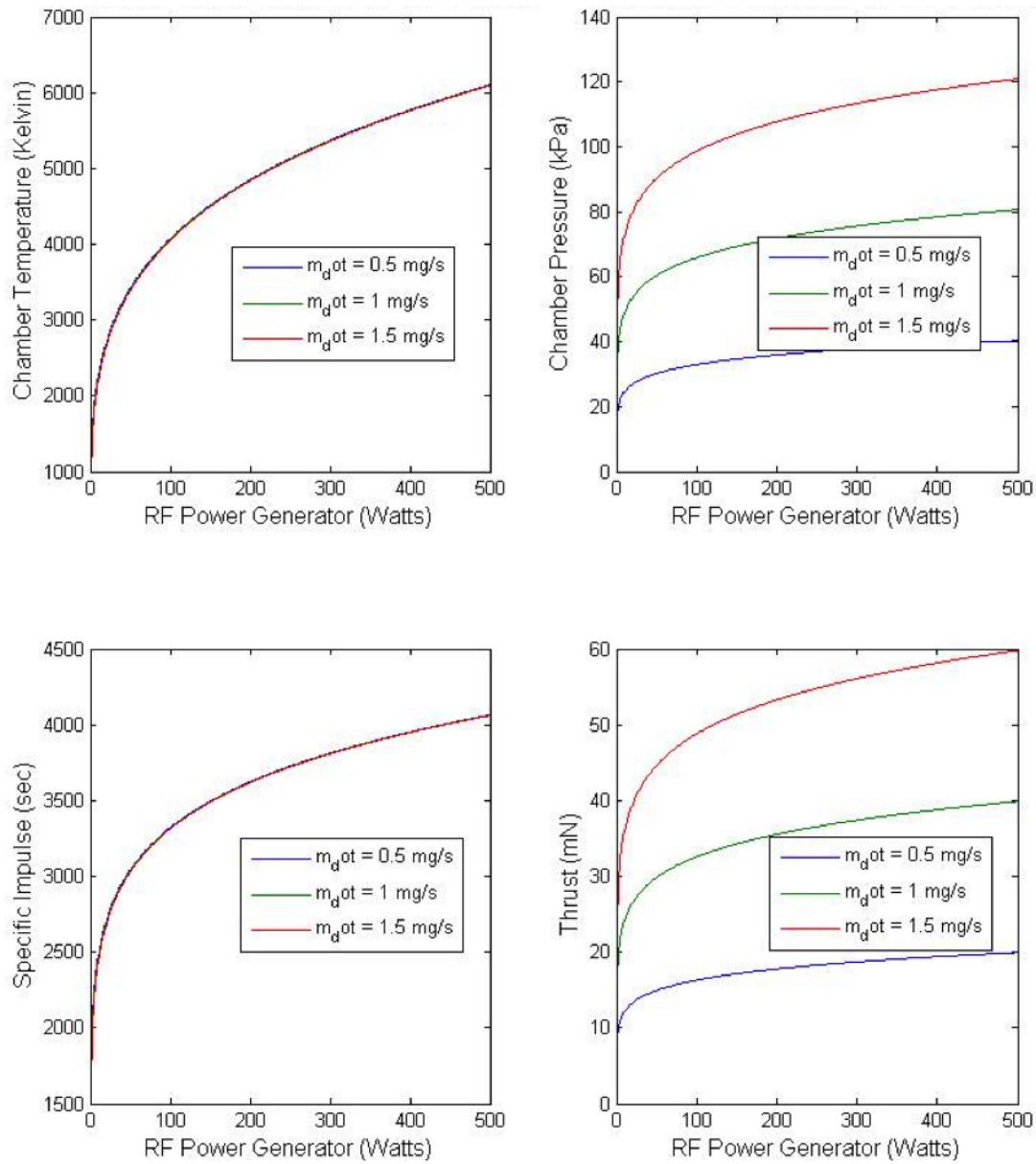


Figure 20. Plots for performance characteristics vs. RF power for the RFET with a throat diameter of 1mm and an expansion ration of 50. Top Left: chamber temperature, Top Right: chamber pressure, Bottom Left: specific impulse, Bottom Right, Thrust.

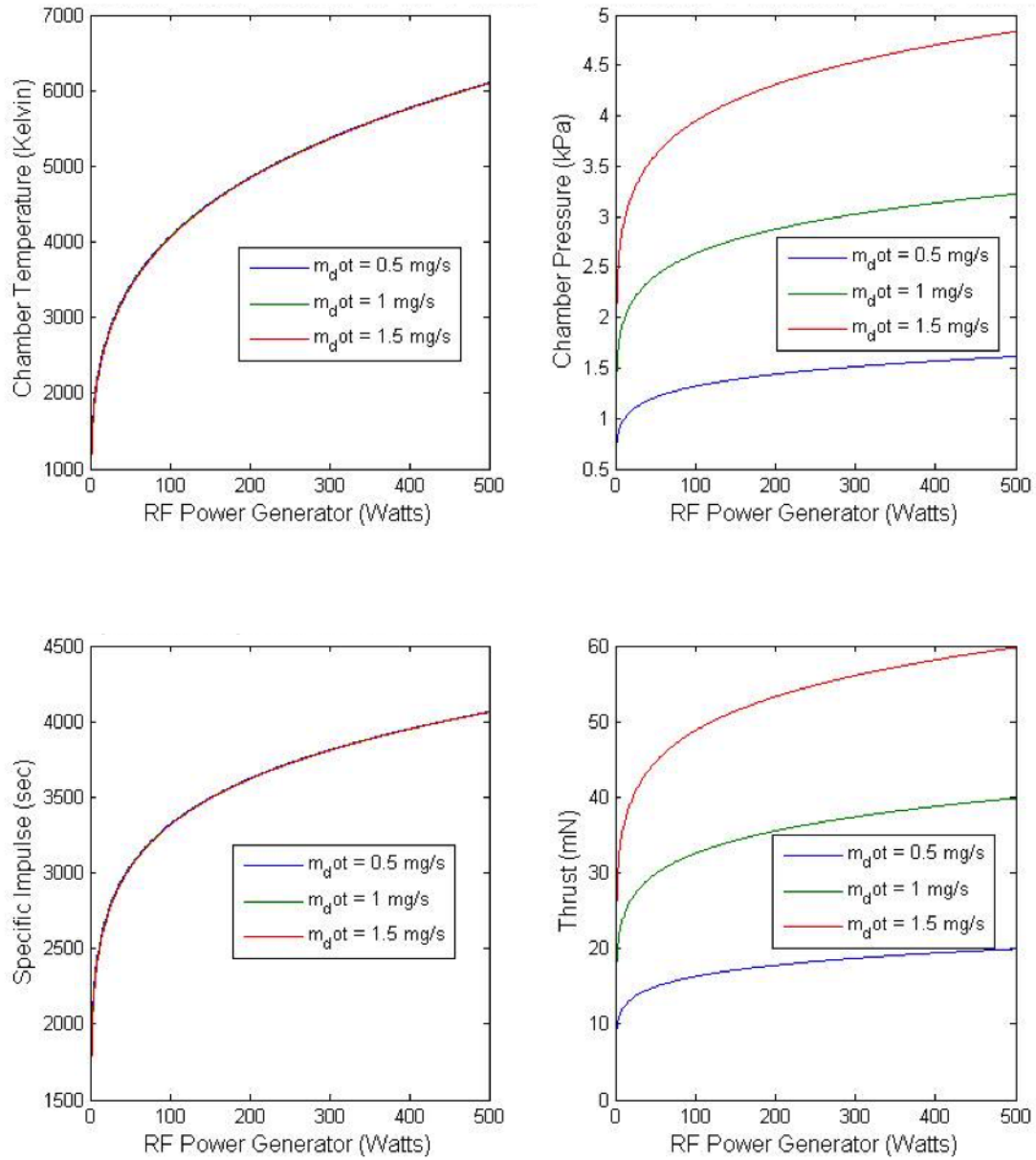


Figure 21. Plots for performance characteristics vs. RF power for the RFET with a throat diameter of 5mm and an expansion ration of 50. Top Left: chamber temperature, Top Right: chamber pressure, Bottom Left: specific impulse, Bottom Right, Thrust.

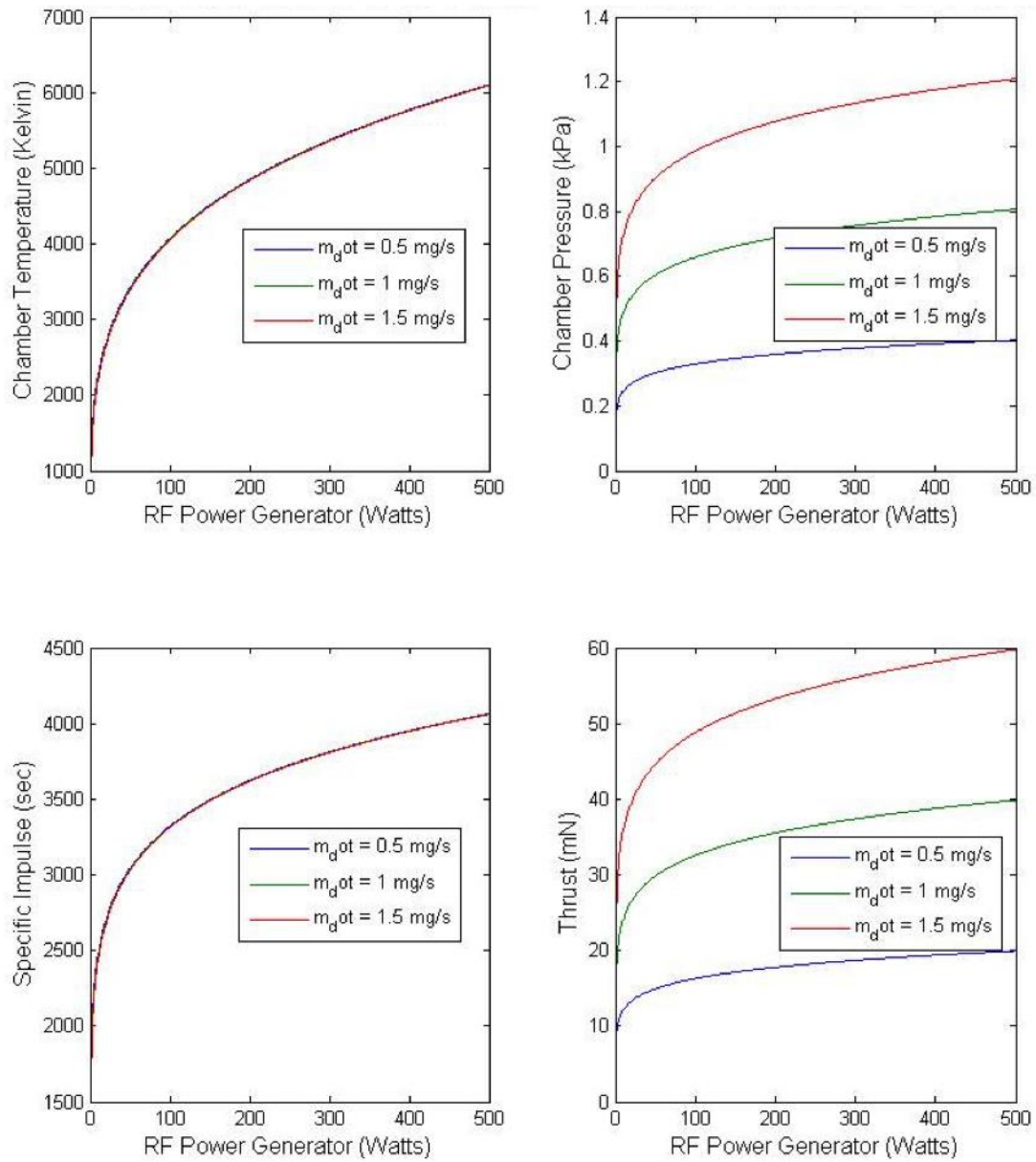


Figure 22. Plots for performance characteristics vs. RF power for the RFET with a throat diameter of 15mm and an expansion ration of 50. Top Left: chamber temperature, Top Right: chamber pressure, Bottom Left: specific impulse, Bottom Right, Thrust.

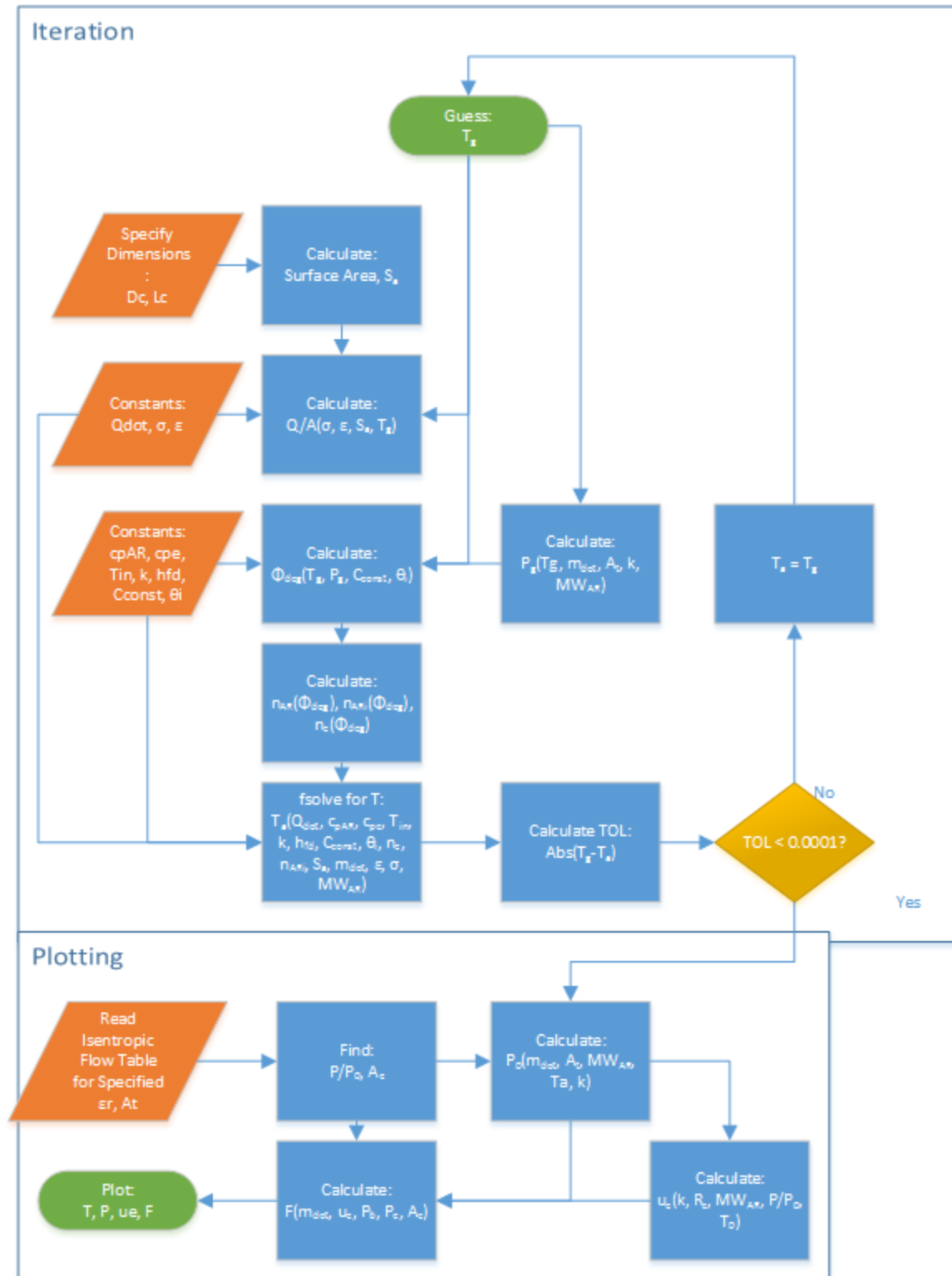


Figure 23. Flow chart for the 0-D MATLAB mass and energy balance model.

The simplicity of the model does result in unrealistic values for the discharge chamber temperatures. While radiation and ionization are taken into account, there model neglects conduction and convection heat losses. In reality the discharge chamber gas temperature is expected to be significantly lower as a large amount of heat transfers to the aluminum housing around the discharge chamber. In this 0-D model, only a single gas temperature is calculated. This is the heavy particle (ions and neutral species) temperature. The heat addition is through a term in the energy balance representing the total power coupled to the plasma. The global model provides no details on the electron collision processes which couple the energy of the hot electrons (with a higher temperature) to the cooler neutral gas [20].

From this model, an expansion ratio of 50 and a throat diameter of 5 mm were chosen, which would keep the pressure relatively low while still producing an adequate amount of thrust and specific impulse. Further, and more accurate, modeling of temperature and pressure was then performed in COMSOL.

3.1.2 COMSOL Model

To a develop a further understanding of the thermal behavior of the thruster, and the RF antenna's influence on the temperature of the Quartz chamber and other components, the CAD model was imported into COMSOL. COMSOL was used to help develop an understanding of the distribution of temperature along the quartz tube, which would allow various parts such as the sealing O-rings, and the housings to be properly placed. In addition, it was hoped that the COMSOL model would help in the selection of optimum materials for particular components.

A transient study was run utilizing both the Solid and Fluid Heat Transfer modules. However, to simplify the simulation and therefore expedite its calculation, only the quartz tube and the argon gas contained within it were analyzed. Below, Table 1 and Table 2 outline the boundary conditions and key parameters for the simulation.

Boundary Condition	Value	Units
Ambient (Vacuum) Temperature	287	K
Ambient (Vacuum) Pressure	0.5	Pa
Power Supplied	500	W

Table 1. Boundary conditions for the COMSOL Simulation

Parameters	Value	Units
Gas Present	Argon	
Material of Discharge Chamber	Quartz	
Surface Emissivity of Quartz	.01	
Mass Flow Rate (Proposed)	0 (1.5)	mg/s

Table 2. Key parameters for the COMSOL Simulation

Because the only parts of the thruster being taken into consideration were the plasma chamber and the supplied flow of gas, there were only two material selections needed, quartz glass for the tube, and argon gas for the flow passing through it. By choosing these materials, COMSOL was able to generate all of the parameters such as heat capacity, emissivity, and

conductivity. The only value which needed to be inputted was the surface emissivity of quartz while calculated the heat dissipated to the ambient atmosphere. This value was chosen to be 0.01 after reviewing plots for surface emissivity of various glass materials [40]. The initial temperature of all components was assumed to be room temperature (287 K).

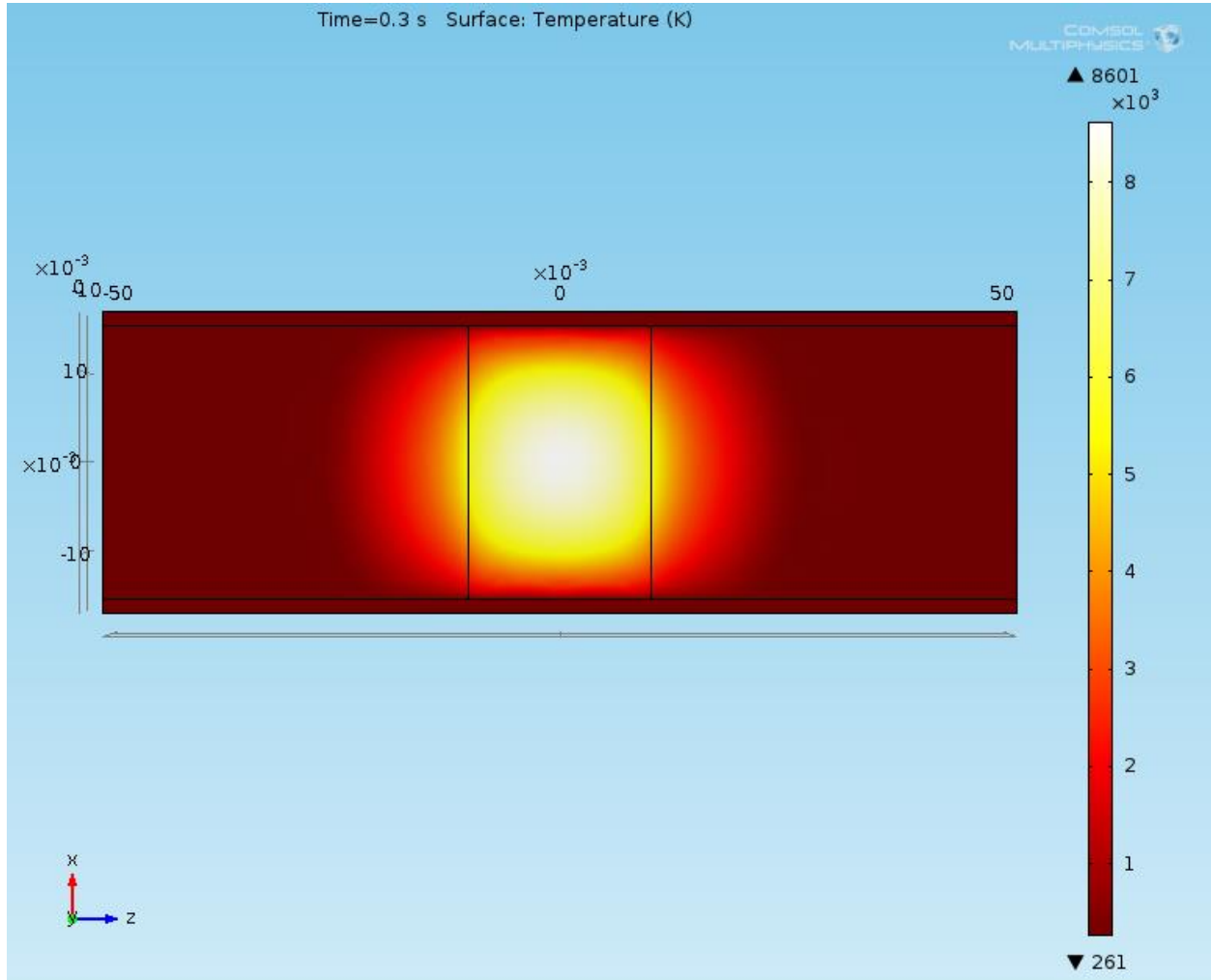


Figure 24. Plot showing a cross section of the Quartz tube containing argon, and the temperature distribution (in Kelvin) found in each while supplied with 500W of RF power.

As the image shows, the expected temperature of around 8000K at 500W concurs with the plots generated from the MATLAB model. However, this simulation accounted only for a

stationary volume of argon. In future iterations of this project, groups may be compelled to add a COMSOL simulation adding Fluid Flow modules to both map the temperature of the flow along the chamber, but also generate more accurate performance values than were calculated in the MATLAB model.

3.1.3 SolidWorks Model

Using the results from the simulations in MATLAB, as well as recognizing the experimental limitations presented by the facilities, the group was able to properly dimension the additional components which will house, secure, and provide argon to the plasma chamber. Initially it was decided to use four threaded rods to attach two square housings together. Holes would be drilled in each corner of the housings, where the rod would be then fed through and secured by nuts to hold the quartz tube in a fixed position. The first pass at a thruster design incorporating housings on either side is shown in Figure 25. This design did not take much into account in terms of sealing the tube and feeding the argon through the housing.

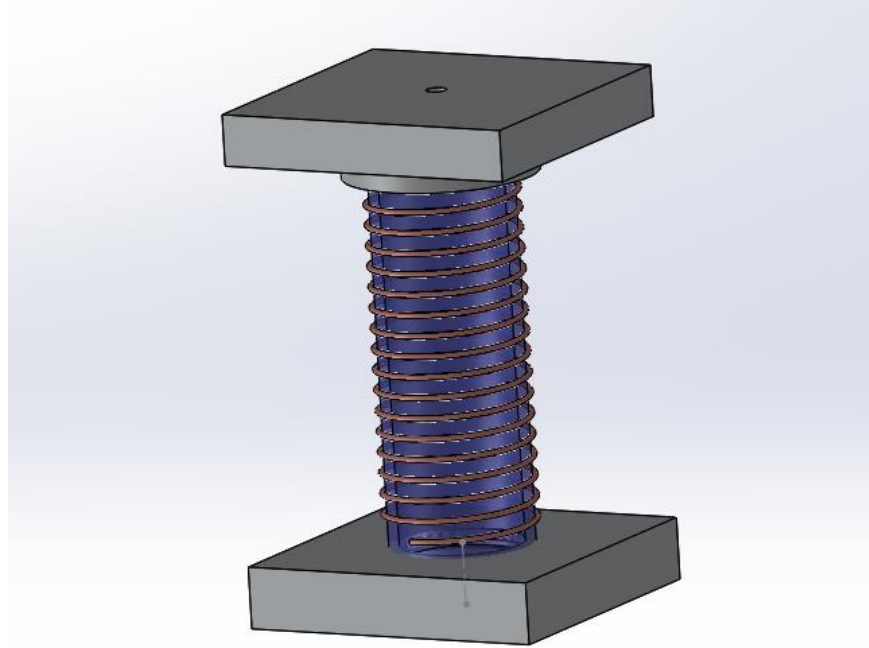


Figure 25. Preliminary design for the RFET Thruster Housings.

The second revision of the design, shown in figure 26, included bolts for holding the housing together as well as a collar to create a compression seal for the o-rings. The most important change was the addition of a removable nozzle plate. The idea was that the thruster could be tested with different nozzles and expansion ratios, or at the very least, it would be easy to replace any nozzles that may melt or be damaged in operation. This was the design that was originally submitted to the machine shop for review.

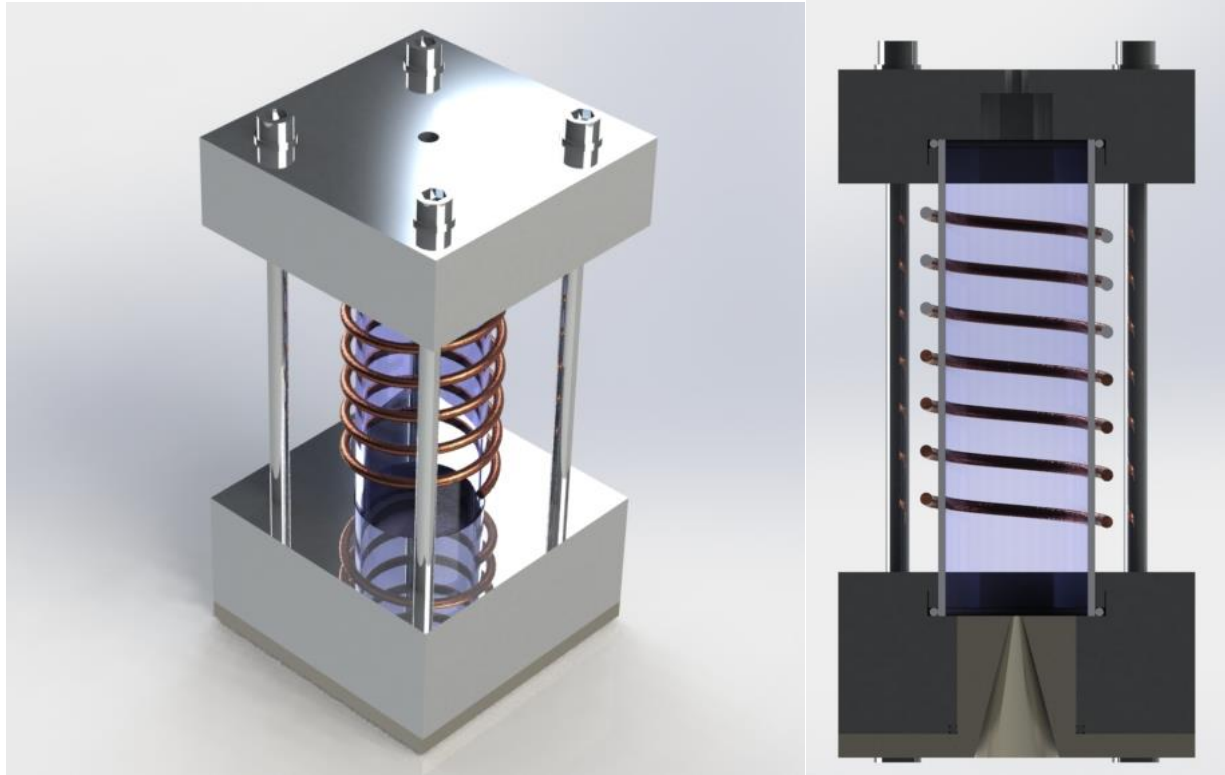


Figure 26. Refined design for the RFET Thruster Housings.

The group then met with Kevin Arruda, the designated Higgins Manufacturing Lab liaison, who advised on how to alter the design to make it more manufacturable, as well as cost efficient. His first suggestion was to move the position of the o-rings, removing the collar and relying on a pressure seal, which would make assembly of the thruster easier as well the manufacturing of the housing simpler. His second suggestion was to add nuts on either side of the thread rod which holds the housings in place. This would prevent the quartz tube from having to bear any stress, and place the role of providing stability solely on the steel rods and housings. Kevin also expressed concern with the manufacturability of the chosen nozzle design, but he suggested the team research alternatives.

After the meeting with Kevin, the new design was taken to the group's advisor. He suggested additional alterations to improve the design, the first of which was to make the housings cylindrical as opposed to rectangular. This would allow for easier manipulation on the lathe, expediting the process of adding grooves and holes for the O-rings and other components. His second suggestion was to increase the girth of the housings, which would permit the threaded rods to be positioned further from the antenna. Professor Blandino expressed concern that if the threaded rods were too close to the RF antenna wrapped around the quartz tube, the RF power could lead to arcing from the antenna to the sharp threads on the rods, proving detrimental to the thruster's efficiency, as well as presenting the possibility of damage to components attached or near the rods.

The manufacturability of the designed nozzle was researched comprehensively, and it was found that the size and shape desired for the purposes of the experiment would be possible if the nozzle were made from graphite. However, to incorporate the nozzle would be too difficult in the time available. It was found that the established design lacked the capabilities to mount the graphite, which is relatively delicate, to the rest of the thruster without damaging the nozzle, or compromising the other components. Therefore, the idea of having a nozzle on the thruster was deferred for a future team, and the idea of a small orifice at the end of the chamber was implemented instead. Figure 27 shows the final design of the thruster, with the round housings, thin nozzle plate, threaded rods and smaller antenna [31]. The changes made to the antenna were done based on recommendations from Dr. Lynn Olson at Busek Co. Inc. based on their experiences working with RF plasma discharges.



Figure 27. Final design of the RFET. Housing diameter of 5" and thickness of $\frac{1}{2}$ in. Support rods are 6 in. long and quartz tube is 5 in. long.

The aluminum housing was sized in two steps. First two identical housings were designed to simplify the machining process. They consist of the concentric holes necessary for holding the tube in place and the support rods to hold the whole thruster together: one center hole designed for each housing, one for the gas feedthrough in the top housing and one for the exhaust and possible future nozzle in the bottom. The outer diameter of 5.0 inches was selected because having a large housing will help act as a heat sink, especially where the o-rings contact both the tube and the housing, reducing the chance of them melting.

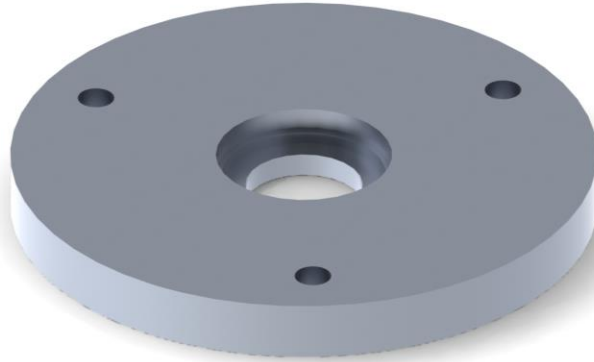


Figure 28. Bottom housing of the RFET.

The concentric holes in the housing were carefully measured to ensure three things. First, if the aluminum expands with the heat of the plasma, it will not compress the quartz tube in any direction. This is why the quartz tube does not contact the aluminum in any spot, either on the face or the end. Next, the hole for the o-ring had to be sized to ensure that the O-ring, while compressed slightly, would not exceed the maximum compression. Because the O-rings are only effective when compressed up to 30% of their thickness [29] and there is a chance of the surrounding aluminum expanding, the hole was sized for 15% compression.



Figure 29. Bottom Housing Cut Away with Quartz Tube and O Ring

The final component of the housing is the bottom “Nozzle” plate. The size of the total plate was designed to be the same as the housing above it, so that it can be attached to the same supports. The plate is significantly thinner than the surrounding housing with only a 1mm exhaust hole.

The thruster was designed to have a modular construction, where each component is easy to replace or modify without changing the entire design. Because of this, as many components as possible are similar while still serving their individual purposes. All of the housing pieces are milled from the same diameter and thickness material, only differing by one small hole. All of the pieces get attached in the same manner on threaded rods. Threaded rods are used instead of bolts because they allow any length, shorter than the rods themselves, of quartz tube to be used without having to acquire new hardware.

The thruster is assembled from the bottom up, with the bottom plate and nozzle being bolted together first. After, the quartz tube with o-ring is carefully set in the groove in the bottom plate. In the event that the snug fit of the o-ring causes it to roll up the quartz tube,

preventing it from sealing to the housing, some form of simple collar or stopper may need to be designed. This should only be temporary, for use while assembling the thruster. The top plate is lowered onto the top of the quartz tube and set in place. Only after the tube is set in both housings snugly are the nuts carefully adjusted and tightened so that the tube is not bearing any of the loads from the housing and there is no possibility of the housing rotating at all. If done correctly, the entire load of the thruster should be distributed between the top and bottom housing via the vertical supports while the tube floats snugly in between.

3.1.4 Material Choices

The biggest factor for material choice for all components was heat tolerance. Because the thruster produces so little thrust and has very little force on it, material strength was less of a concern. Most of the components come into contact with very high temperature gas and thermal expansion, cracking and melting is a strong possibility.

The component that is exposed to the greatest increase in temperature will be the tube that has the antenna wrapped around it. A large amount of RF power passes through the tube and the gas inside will be excited to a high temperature. Because of this, a quartz tube was chosen over a regular glass tube. This decision was made based on the recommendation of numerous other RFET thrusters, especially the Penn State one [1]. Quartz was chosen because of its ability to handle high temperature without cracking and its extremely low coefficient of thermal expansion, $5.5 \times 10^{-7} \text{ cm/cm } ^\circ\text{C}$. In addition, the tube does not start to soften until it reaches 1683°C . This means that with regards to temperature, this should be the last component to fail. The one drawback with the quartz is that it is fragile, meaning compressive

forces could cause it to shatter easily. This has already been discussed in reference to the thruster assembly procedure.



Figure 30. Antenna Wrap on Quartz Tube

The next component for which heat load is a significant concern is the o-ring which seal the quartz tube to the outer housings. The O-rings are in constant contact with the tube, which is expected to heat up. Because of this, normal Burna-N o-rings would not be rated to a high enough temperature. Their seal is only good to between 212 and 250 degrees Fahrenheit. Instead Viton® Fluoroelastomer o-Rings were chosen, because their seal is good to 400 degrees Fahrenheit. Although o-rings that are rated to high temperatures are available, they were out of the price range for the project.

The housing on either end of the quartz tube has a bit less of a thermal concern, as compared to the tube itself and the o-rings, but also has machinability and cost concerns. Because a material was needed that had could withstand the high temperatures of the thruster without melting, while being easy to machine, Al 6061 was chosen. While stainless steel might have been a better choice due to its high melting point (~2600 °F compared to Al6061 at ~1200 °F), the increase purchasing cost and difficulty in machining ruled it out for this project.

The remaining hardware is all stainless steel. It was chosen because of its strength and excellent thermal properties, while not being significantly more expensive than the aluminum alternatives in the quantities that are needed.

3.1.5 Gas Feed In

To ensure that the argon gas is fed into the quartz tube and does not leak into the surrounding vacuum, a Swagelok Tube Fitting, Bulkhead Male Connector is used. The fitting will seal around the top housing and to the 1/8" tube that is feeding the gas. The open end terminates in a male NPT end, but it is not being used, it is just opening into the quartz tube. The entire fitting is made of stainless steel to that it can handle the possible heat of the discharge chamber. In the compression seal, a ferrule in the top nut clamps down on the gas hose, ensuring a tight seal, which the two middle nuts tighten down on either side of the housing, creating a tight seal.

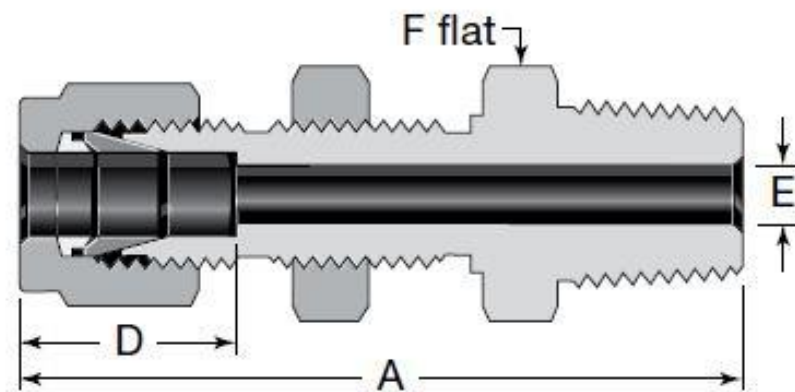


Figure 31. Swagelok Tube to Male NPT Bulkhead Fitting. [30] © 2009, Swagelok.

3.2 Assembly

3.2.1 Acquisition of Materials

The process of fabricating and assembling the thruster began with the acquisition of the parts necessary to build it. Fortunately much of the materials, such as the 5/16th threaded rod and its corresponding nuts and washers were already available. However, the quartz tube had to be ordered, as did the aluminum for the housings as there were no pieces large enough for our purposes, and it had to be of a specific geometry. The Swagelok fitting which introduced the mass flow to the thruster also had to be ordered. The quartz tubing was ordered from GlassProducts.com [22], the aluminum sheets from MSC [30], and the Swagelok from the company's website [34].

3.2.2 Fabrication of Components

First, the threaded rod was cut into three seven inch sections. Then, the aluminum plate, which came with 12x12 inch dimensions, was cut into four 6x6 squares, two for the housings, one for the CNC mounting plate, and a spare. Fortunately, the quartz tubing was able to be ordered precut at 5.0 inch lengths. The next step was to machine the housings out of the aluminum plates. Due to the tight tolerances, as well as difficulty of the necessary cuts, Computer Automated Manufacturing (CAM) had to be utilized. A picture of the aluminum plates, ready to be machined is shown in Fig. 32.

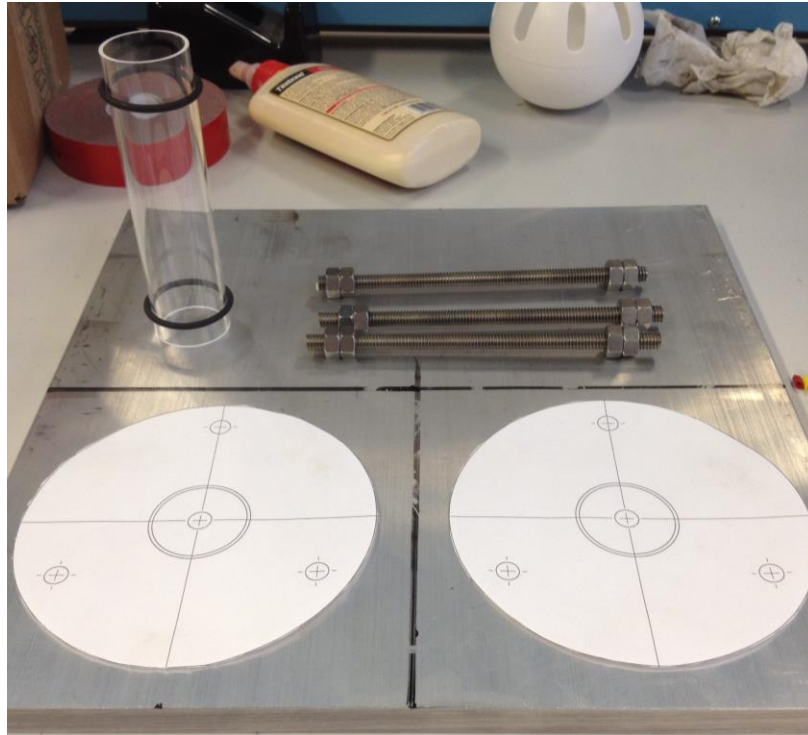


Figure 32. Aluminum Plate ready to be machined.

The drawings for either housing were imported into Esprit (DP Technology Corp. Camarillo, California), where their faces and surfaces were identified for cutting paths. The first CAM file written was one that would only drill the three holes for the threaded rod, with a diameter slightly smaller than the rod. These were to be tapped after the CNC code was run using the Haas Minimill in the Higgins Machine Shop. The holes for the housing were then drilled as well, using the same code but a different bit. Next, the CAM files for the CNC cuts for the outer perimeter, and inner surface were generated and exported for use in the Minimill. The plates to be milled into housings were then screwed to the mounting plate with three bulk head screws to secure it, and the CNC program was run. However, for the second housing, which was to be the bottom, the machining was stopped before the final drill (the center hole)

was made. This is because the hole on the bottom was to be 1 mm in diameter, and had to be done by way of a manually controlled mill. Once the two circular housings were milled, they were removed from the mounting plate and combined with the quartz tube and threaded rods to create the finished structure, shown in Fig. 33.

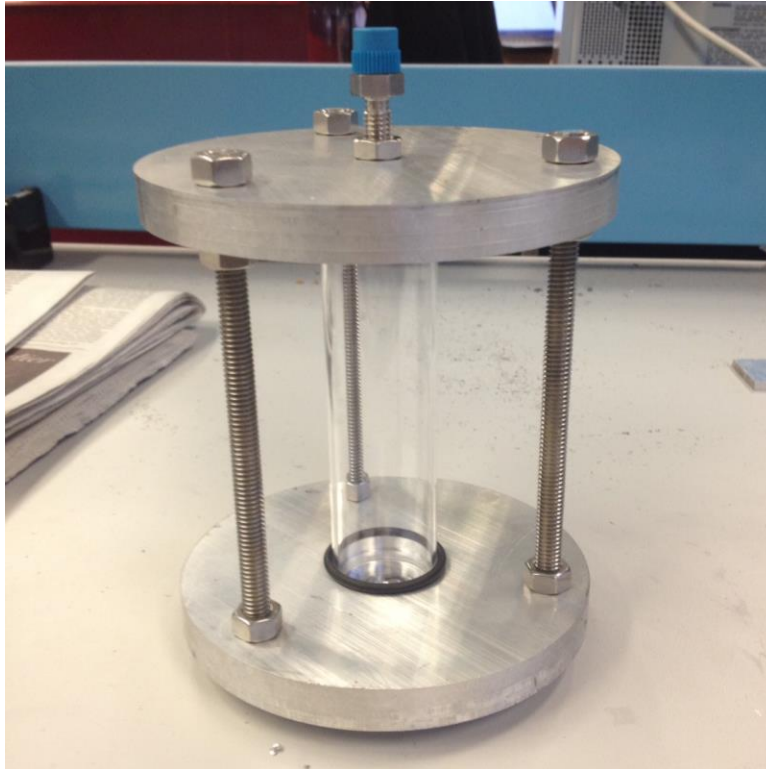


Figure 33. The final machined and assembled thruster.

3.3 Test and Facility Integration

In order to be able to test the device in the T4 Vacuum Chamber, a number of tasks needed to be completed. The thruster relies on a gas feed and RF power. Because the argon tank and RF power source are outside of the vacuum chamber, feedthroughs are required to get the coaxial cable and gas line inside the chamber. Another necessity was to vent the exhaust from the mechanical pump to outside. For safety reasons, there was also the need to

run the argon exhaust outside through a rubber hose instead of just venting into the lab. Other tasks required for the integration included moving the RF power source from by the T2 chamber to near the T4 chamber. A matching network also needed to be designed and incorporated into the circuit. This also involved redoing the coolant lines for the power supply. The argon tank needed to be placed by the T4 tank as well as the gas flow control panel previously installed near the T2 vacuum chamber.

T4 Vacuum Chamber Test

Since the T4 chamber had not been used for roughly 8 months, an initial test was completed to check for leaks and proper operation. These results would be useful later when the gas and power feedthroughs were installed. This information would explain whether or not the installed feedthroughs were the cause of a leak or if the leak was present beforehand. The chamber, which was still in a partial vacuum at roughly 2.0 Torr, was pumped down to 27 mTorr and a Rate of Rise (ROR) test was completed using the procedure outlined in Appendix A.1 of reference [14]. Table below outlines the results.

Start Pressure (mTorr)	Stop Pressure (mTorr)	Duration (min)	Rate of Rise (mTorr/min)
27	39	17	0.71

Table 3. Rate of Rise Test

The results from the ROR test were very encouraging and showed that the chamber was in good operating condition with minimal leaks. An acceptable value is anything less than 5 mTorr per minute. After the ROR test, the chamber was further pumped down using the

Turbopump. It was allowed to pump for 2.5 hours until we were satisfied that everything was operating well. The final pressure achieved after 2.5 hours was $5.9\text{e-}6$ torr or $7.76315\text{e-}9$ atm. Since this is lower than our intended testing pressure, the test was ended and the data recorded in the T4 chamber notebook.

3.3.1 Impedance Matching Network Design

As discussed in the background, an impedance matching network is required in order to ensure a high percentage of transmitted power reaches the discharge chamber. After speaking with Professor Reinhold Ludwig in the Electrical and Computer Engineering Department at WPI, a basic plan was established. An L-type matching network was recommended due to the simplicity. However, the biggest foreseen issue was the load of impedance (of the discharge chamber) knowing that this value would change with time, gas flow rate, chamber pressure and input power. A starting point, or estimate for this load impedance was needed. The argon impedance data discussed in the background section was crucial here as it gave a range of resistance and reactance that could be used as a baseline for design of the matching network. The only issue with the data provided by reference [28], is that their experiment's power input ranged from 500 to 5000 watts. This RFET thruster would be using a RF power source with input power ranging from 50 to 650 watts. The data provided by reference [28]'s graphs was used in order to plot the same data in Excel. Then, power curves fits were added to the data points with R^2 values above 0.97, so that the trends below 1000 watts of RF power could be observed. This is seen in Figures 34 and 35, below.

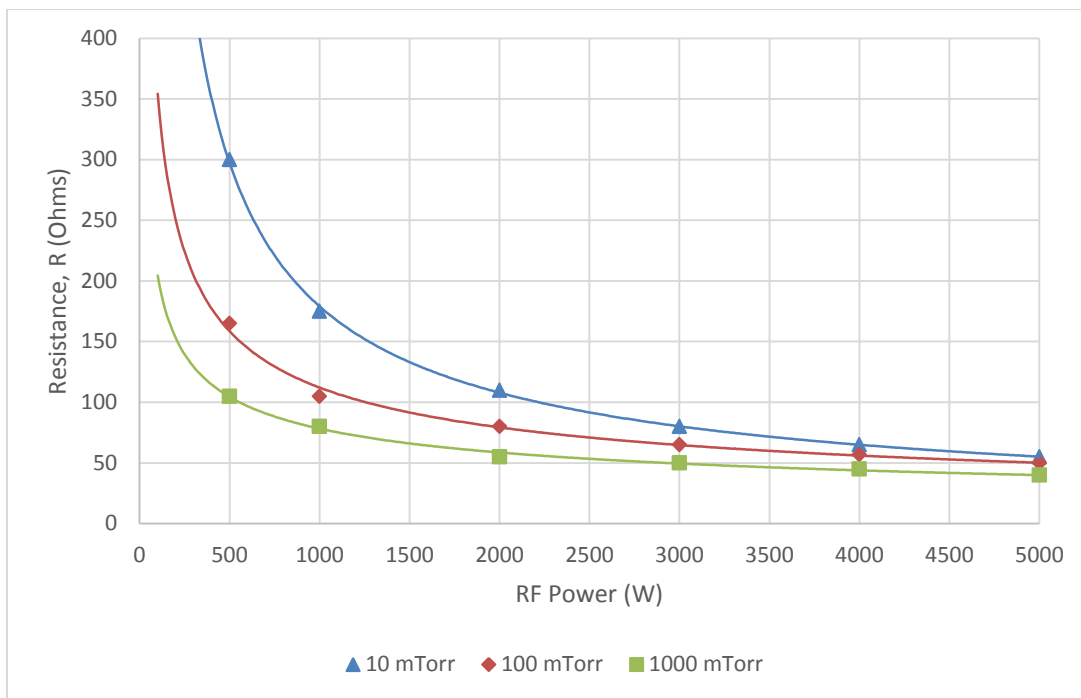


Figure 34. Resistance vs. RF Power for Different Argon Pressures

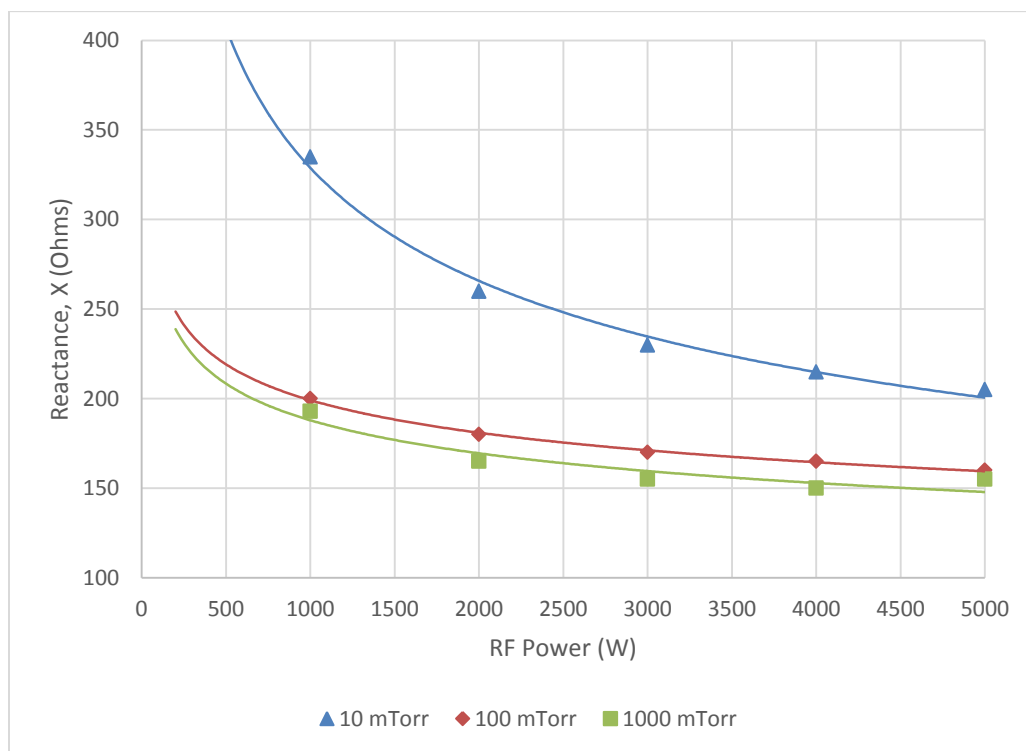


Figure 35. Reactance vs. RF Power for Different Argon Pressures

These plots provide the data necessary to make estimates as to what the impedance values would be for the proposed RFET setup. In the same Excel spreadsheet, the formulas for the lines of the impedance graphs above were entered so that the resistance and reactance could be quickly calculated by just inputting the pressure. This was then continued to calculate the reflection coefficient, Γ_L , through Eq. (15) below.

$$\Gamma_L = \frac{\sqrt{(R_L - Z_s)^2 + X_L^2}}{\sqrt{(R_L + Z_s)^2 + X_L^2}} \quad (15)$$

With the reflection coefficient, the power reflected and the power transmitted can be calculated, based only on the input power and the reflection coefficient. The power transmitted, P_L , can be calculated from Eq. (16) where P_{in} is the input power from the power supply [26].

$$P_L = P_{in}(1 - |\Gamma_L|^2) \quad (16)$$

For the power supply being used for this setup, the max input power is 650 Watts. So, using these formulas and the impedance data, the percent power transmitted for input powers ranging from 50 to 650 Watts was plotted. Figure 36 displays this information.

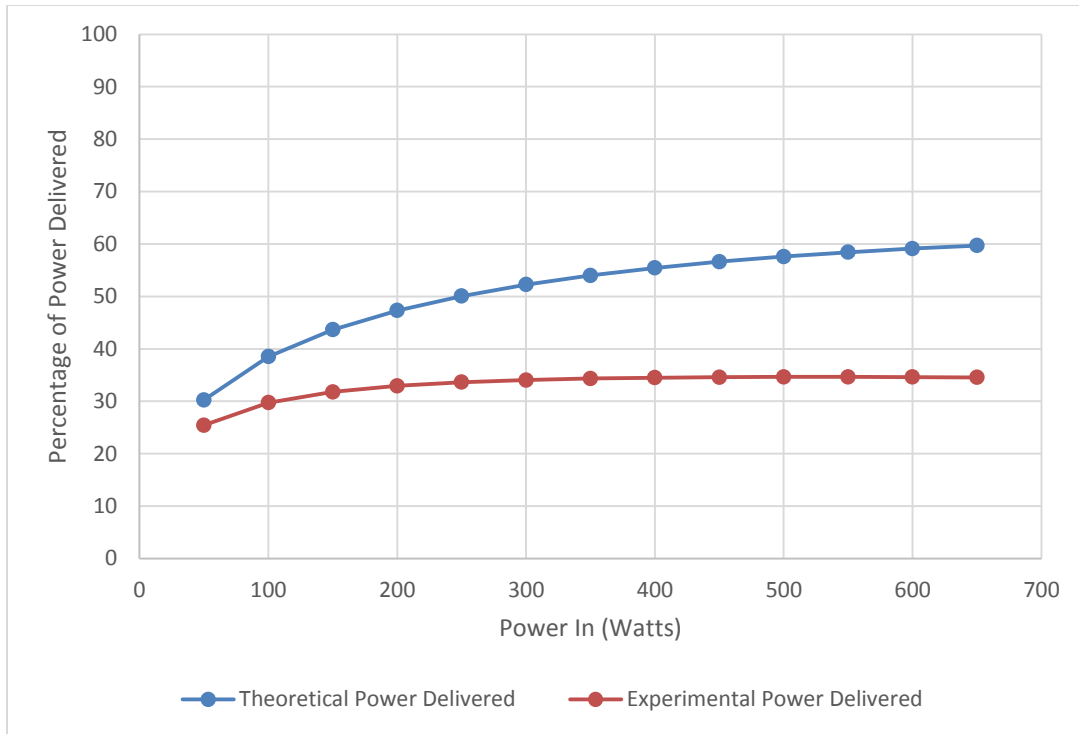


Figure 36. Percentage of Power Delivered vs. Input Power (Unmatched Network)

The orange “experimental” line represents the percentage of power transmitted by using the load reactance and resistance provided in the plots for argon provided by reference [28]. The blue line represents a theoretical approach using equations 2 and 3 for X_S and X_L discussed in the background section on matching networks. These calculations include both this theoretical and experimental data in order to provide a better understanding of the ranges needed in the matching network. If the constructed matching network can accommodate the range of both the theoretical and experimental impedances that are possible, for the network will be more likely to correct for changes in operating conditions and other uncertainties.

The Excel spreadsheet was then used to calculate the values for the capacitor and inductor, C and L, needed in order to match the impedance of the load and source. This was

also done using both theoretical and experimental data. The formulas used in the Excel spreadsheet are the same presented for C and L in the background section on matching networks. The inductance does not change between the theoretical and experimental setups because L only depends on X_s , which is the same in both the theoretical and experimental setups. The impedance of the source is a fixed, and known value. However, the capacitance does change between the theoretical and experimental calculations. Then, the needed capacitance and inductance to match the impedance for input power ranging from 50 to 650 watts is plotted in Figure 37.

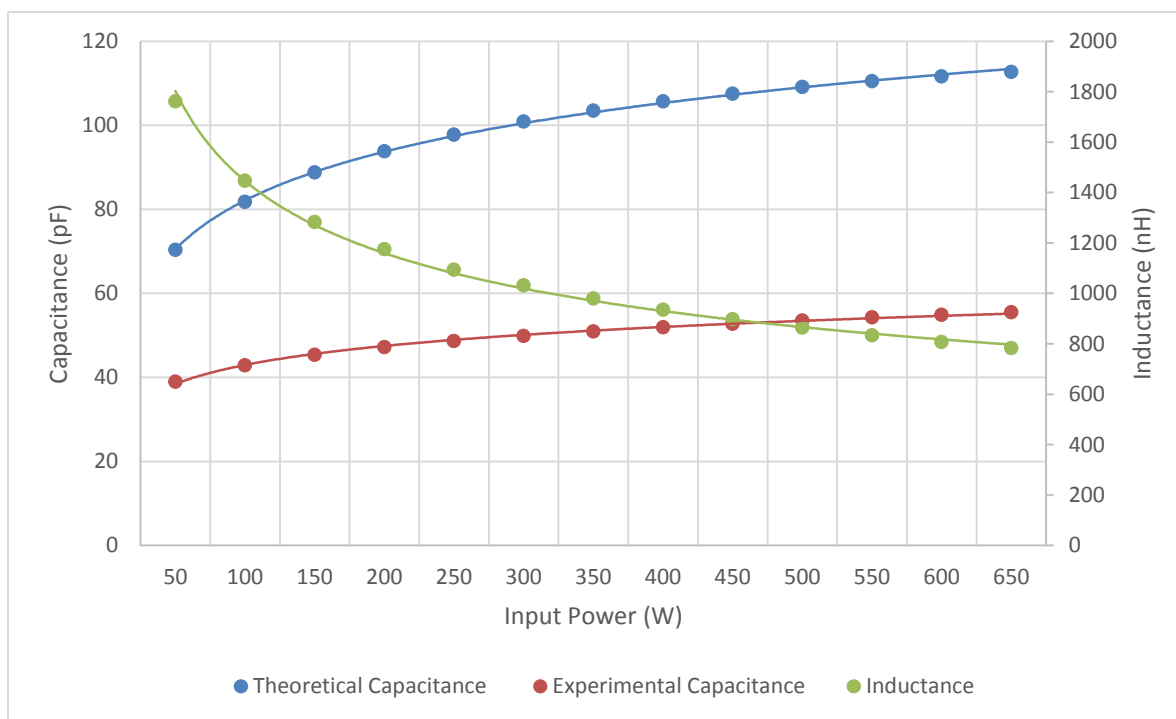


Figure 37. C and L values to Match Impedance vs Input Power at 100 mTorr

This chart provides a good visual representation as to what is required as far as capacitors and inductors in order to match the network for a chamber pressure of 100 mTorr. This chamber pressure was used due to being middle ground and easily achievable to maintain

with the mass flow rate capabilities of the T4 vacuum chamber. Since a variable capacitor is to be used in the matching network, it appears that a capacitor that can vary from about 40 pF to 120 pF would cover the possible ranges of impedance for all possible pressures at both the theoretical and experimental states. The inductor sizing, however, is a little more difficult. This is due to the fact that variable inductors are not as readily available as variable capacitors. In addition, the variable inductors that are available have very low ranges (such as ± 10 nH) and having relatively low durability with high voltages and currents. For this reason, a fixed inductor is used in the matching network. This means that the network will likely never be completely matched, but will greatly increase the power transmitted nevertheless.

After examining available inductors that could handle high currents and voltages and cross referencing those with Figure 37 calculations were performed with an inductor with an L value of 1200 nH or 1.2 μ H. Using this and a variable capacitor that covers the possible ranges of impedance that could be experienced, another plot was created for the percentage of power transmitted when using this matching network at a chamber pressure of 100 mTorr. This was calculated exactly as before, with the reflection coefficient equation given above (Equation X). The only difference is that reactance, X_L , is negated and the resistance, R_L , is reduced. These calculations are plotted below.

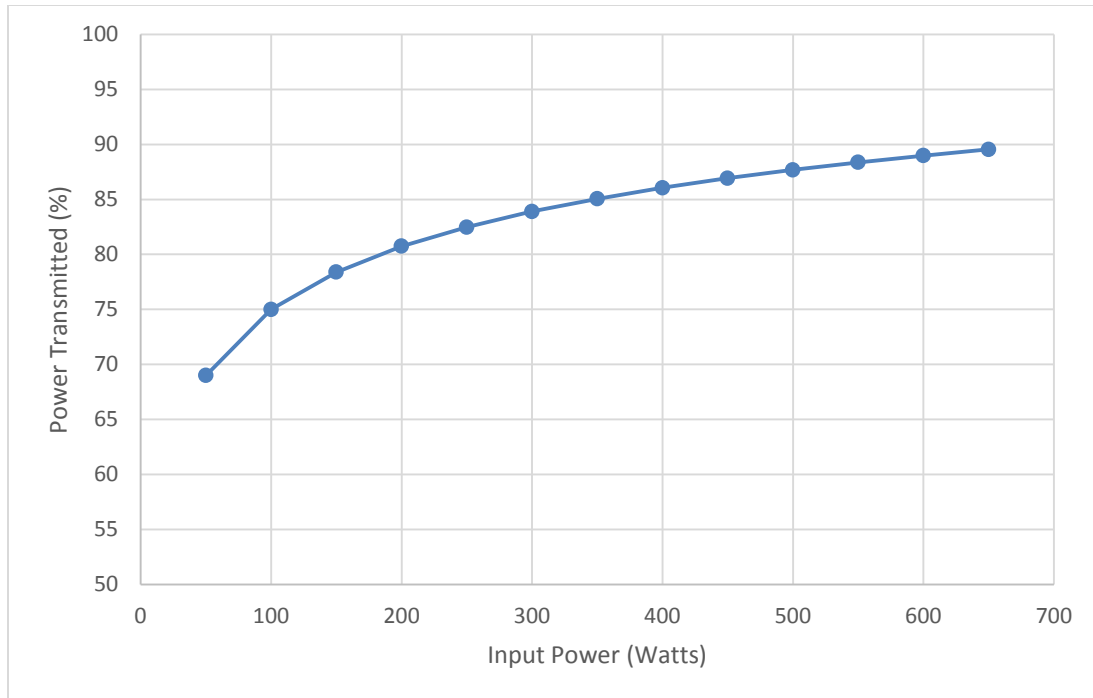


Figure 38. Percentage of Power Delivered vs. Input Power (Matched Network)

This data is very encouraging because at 300 Watts of input power, almost 85% of power is delivered to the discharge chamber. This is a substantial improvement over the 35% delivered with the unmatched system and is sufficient for the purposes of this project.

3.3.2 Matching Network Component Selection

The selection of components for the matching network was completed after the calculations and designing were complete. The necessary components for the matching network include a chassis (or electrical box), coaxial cable, a variable capacitor, an inductor, a knob for the capacitor, grounding cables and type-N chassis connectors for the coaxial cable. The capacitor was selected first. The search was for a variable capacitor that had a range of capacitance from roughly 40 pF to 120 pF that could handle high voltages and currents. RF Parts Company (www.rfparts.com) had a lot of options for radio frequency components [33].

They carried a plate style variable capacitor that's capacitance ranged from 14 pF to 145 pF and voltage capabilities of up to 2500 V. This range covered the needed range and still provided an extra buffer on the both ends of the range. Using goal seek in the Excel spreadsheet, there was no solution for the impedance that would result in the required capacitance lying outside of the range provided by this capacitor. In other words, according to calculations, this capacitor will always be able to match the load impedance for our setup. The capacitor is pictured below in Figure 39.

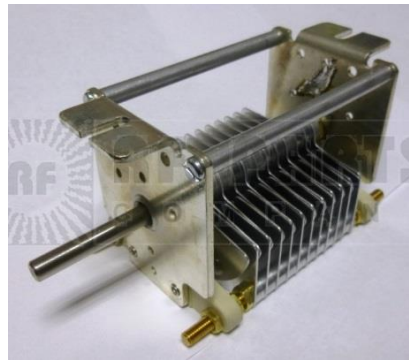


Figure 39. Capacitor [33] © 2015 RF Parts Company

For the inductor, the search also was for components with high current and voltage ratings. Coil WS carried a wide selection of ferrite based inductors with inductance values in the range we needed [35]. These also had very high current ratings of 40 amps. An example of one of the Coil WS inductors is shown in Figure 40.



Figure 40. Inductor [35] © 2008 Coil WS

As far as sizing the inductor, a few options are available. The range for inductance provided from the data is from 0.8 μH to 1.7 μH . As the ideal operating input power for the thruster is 300 W, a 1 μH inductor is recommended as that is the required inductance to match the impedance at 300 W. However, because of the high probability of unforeseen changes in impedance and differences in setup, having multiple inductors available provides some flexibility. Three inductors were purchased, with inductance values of 0.6 μH , 1 μH , and 2.10 μH . These are all available from Coil WS and provide a comprehensive range of inductance to combat unforeseen changes in matching network requirements. These could be easily switched out by using spade connectors.

The enclosure, coaxial cable chassis connectors, and dial were also all found with the RF Parts Company. The chassis connectors will be secured onto the enclosure in order to plug the coaxial cable from the power supply into the matching network as well as to connect the matching network to the vacuum chamber. These are pictured in figure 41.



Figure 41. Chassis Adapters [33] © 2015 RF Parts Company

A standard dial was selected to adjust the variable capacitor from outside the box. A basic aluminum enclosure was also selected to house the matching network.

The coaxial cable used is also very important. A key element to this is the length of the cable running from the power source to the matching network. As discussed in the background section on the matching network, this length should be equal to a quarter of the wavelength. The RG223 cable was selected for the project. This was selected after researching coaxial cables and contacting customer service at Pasternack [37]. Pasternack is a large supplier of RF cables and was able to recommend the RG223 cable for our given setup. This was mainly based on the power handling abilities and cost. This cable can handle 800 watts at 13 MHz, comfortably covering our max operating power. After selecting the cable, the velocity factor was found to calculate the quarter wavelength. The velocity factor for RG223 cable is 0.66. The formula for λ given in the background section on matching networks is used in Eq. (17) to calculate the total wavelength and quarter wavelength.

$$\lambda = \frac{(3.00 \cdot 10^8)}{(13.56 \cdot 10^6)} * 0.66 = 14.6 \text{ meters} = 47.9 \text{ feet} \quad (17)$$

$$\frac{1}{4} \lambda = 11.975 \text{ feet}$$

Here, it is seen that a cable length of 11.975 feet is required to connect the power source to the matching network. This cable can be purchased from Pasternack at custom lengths with Type-N connectors. Another, shorter 3 foot section of this cable with Type-N connectors is used to connect the matching network to the Type-N feed through on the vacuum chamber. Some RG223 cable with no connectors was also selected in order to use as cable inside the matching network. An example of the cable and Type-N connectors can be seen in Figure 42 below.



Figure 42. Type N Connectors [37] © 2015 Pasternack

Another component required for the matching network circuit is a cable to establish a proper ground connection. Metal braided grounding cables are very durable and highly conductive, ensuring a stable and effective ground. This is very important since this project requires the grounds for the matching network and the vacuum chamber to be connected with a very reliable connection to avoid charging of the chamber or other facilities. Two of these are needed in order to ground both the chamber and matching network. A 30 inch stainless steel

grounding strap sold by Summit Racing Equipment was selected for its relatively low cost and sufficient length [36]. Table 4 summarizes all of the components selected for the impedance matching network.

Company	Item #	Item Description	Qty:	Unit Price (\$)	Total Price (\$)
RF Parts	73-175-23	Variable Capacitor 14-145 pF	1	54.95	54.95
RF Parts	CHAS1444-24	Enclosure/Chassis	1	26.15	26.15
RF Parts	172119	Chassic Connectors (type N)	2	4.95	9.90
RF Parts	KNOB16	Turning knob	1	3.95	3.95
Coil WS	CWS-37819	1.0 uH Inductor	1	7.50	7.50
Coil WS	CWS-35067	0.6 uH Inductor	1	7.00	7.00
Coil WS	CWS-39206	2.1 uH Inductor	1	7.00	7.00
Pasternack	PE3447-144	144" RG223 Cable with Type N Connectors	1	66.01	66.01
Pasternack	PE3447-36	36" RG223 Cable with Type N Connectors	1	41.75	41.75
Pasternack	RG223/U	RG223 Coax Cable (1 foot)	3	2.43	7.29
Summit Racing Equipment	28135	30" SS Grounding Strap	2	16.97	33.94

Table 4. Matching Network Components

3.3.3 Facilities Integration

RF Power System

The radio frequency power source provides the power for the thruster. It is a model ENI OEM-650A RF Plasma Generator built by ENI. The power supply was previously installed in an

electronic rack located next to the T2 vacuum chamber and therefore needed to be moved to the T4 chamber. Because this power supply requires liquid cooling, the coolant lines also needed to be extended over to the new location by the T4 chamber. This meant that more coolant hose needed to be purchased in order to reach the T4 chamber from the wall connection for the liquid coolant. The same type of hose that was already being used was purchased along with a couple of brass push-on hose fittings (McMaster Carr Item # 91465K51) so that the hoses could be connected. Thirty feet of this Buna-N green hose with a ½ inch inner diameter (McMaster Carr Item # 5288K13) was purchased. These products were purchased from McMaster Carr [34].

Another important component for the integration of the power supply in the T4 chamber is a Type-N feedthrough for the vacuum chamber. These are very expensive components, costing approximately \$375 for a double-sided Type-N feedthrough. Luckily, the Busek Corporation of Natick, Massachusetts allowed the group to borrow a Type-N feedthrough on a Conflat (CF) 2.75 inch flange. Unfortunately, the T4 chamber did not have any CF flanges installed, so an adapter was required. A KF-50 to CF 2.75 adapter was selected from Ideal Vacuum Products (Item #P101966) [38]. This solution saved almost \$300 that would have been required to purchase the Type-N feedthrough on a KF-50 flange. The feedthrough, provided by the Busek Corporation, and the flange adapter are pictured in Figures 43 and 44.



Figure 43. Feedthrough - Property of Busek Corporation, Inc.



Figure 44. Feedthrough Adapter [38] © 2014 Ideal Vacuum Systems

Gas Flow System

The gas system was also previously set up for use in the T2 chamber. To move it required moving the control panel as well as the regulator and argon tank. The flow control panel was mounted next to the T2 chamber as shown in Figure 45.

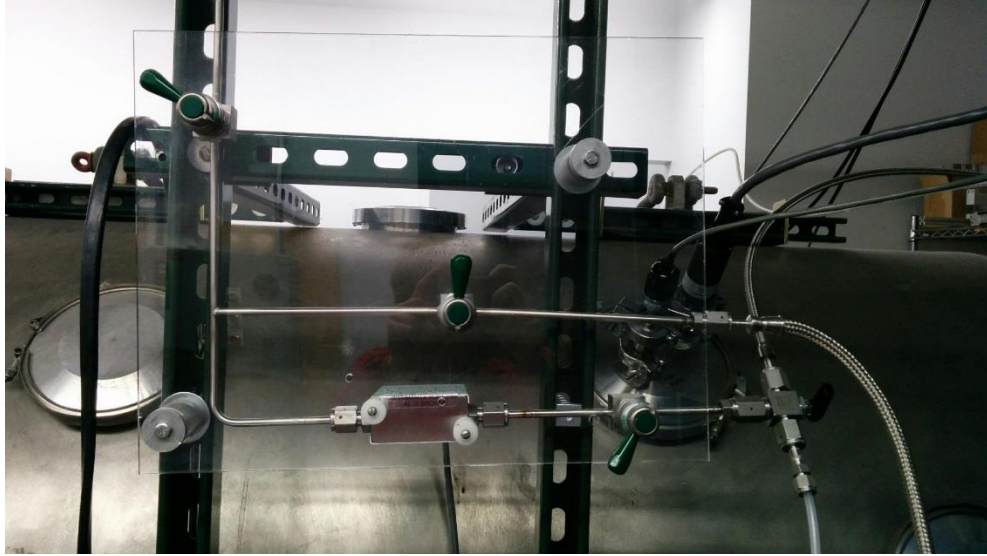


Figure 45. Picture of T4 Chamber

The flow panel was then moved and reinstalled in the top of the electronic rack to the left of the T4 chamber. The argon bottle was also repositioned to the back of the T4 chamber. The final positions of these are seen in Figures 46.

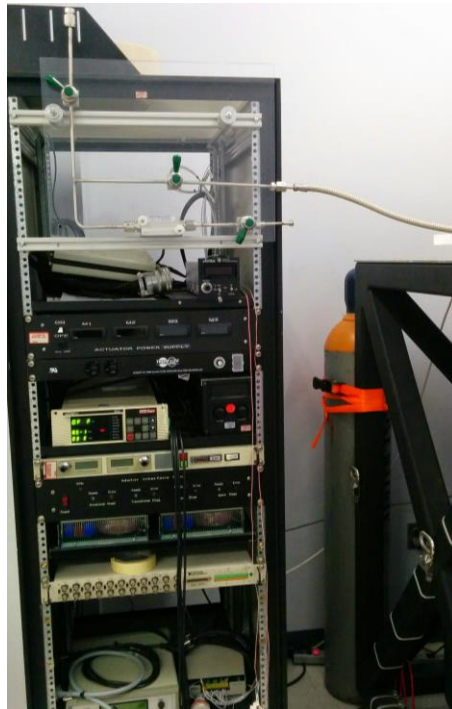


Figure 46 Flow Control and Argon Tank In Final Location

In addition, the power supply can be seen in the Figure 47.



Figure 47 ENI OEM-650A RF Power Supply

Also required for the gas flow system was a feedthrough for the gas to enter the vacuum chamber. For this, an NW-50 1/4" FNPT pipe adapter feedthrough was purchased (Item # NW50-1/4FNPT) from the Vacuum Research Corporation [39]. This was used with a 1/4" Swagelok bulkhead bored-through fitting (Item #SS-400-11-4BT) purchased from Swagelok to get the gas tube inside the vacuum chamber [30]. These are both pictured in Figures 48 and 49.



Figure 48. NPT Fitting [30] © 2015 Swagelok



Figure 49. NPT Feedthrough [39] © 2015 Vacuum Research Corporation

Exhaust Flow System

The exhaust system from the mechanical pump of the T4 vacuum chamber also needed integration for testing. Since argon gas will be pumped out of the chamber during operation of the thruster, a safer system for the exhaust was devised. An NW-25 rubber hose adapter (Item # NW25-HOSE.75) was purchased from the Vacuum Research Corporation in order to attach to the output of the mechanical pump on the T4 chamber [39]. This adapter is shown in Figure 50.



Figure 50. Hose Adapter [39] © 2015 Vacuum Research Corporation

To ventilate this exhaust out of the lab, a contractor grade garden hose was selected from Home Depot (Item # 202210362) to run from the above adapter to outside through the loading bay. Worm-drive hose clamps were also purchased from McMaster Carr to secure the hose on the hose adapter.

Thruster Mounting Stand

In order to mount the thruster in the T4 vacuum chamber, a stand needed to be designed and built. At the bottom of the chamber, there is a collar with a 13.6cm hole. This is the main opening for all pumping operations, so it cannot be blocked. Because of this, the thruster must be mounted on a stand of sorts that spans the hole without impeding air flow.

The thruster mount consists of four 3 inch legs, connected by 8 inch cross beam and 12 in supports. On top of the long supports, there are a series of four L brackets, to hold the thruster to the stand. This takes advantage of the threaded rod running through the length of the thruster, connecting to two of them, ensuring that the load of the thruster is placed on the rods and not on the quartz tube. Figure 51 shows thruster stand, the locations of the attachment points and the mounting hardware. Figure 51 shows how the thruster attaches to the stand and what the entire assemble looks like.

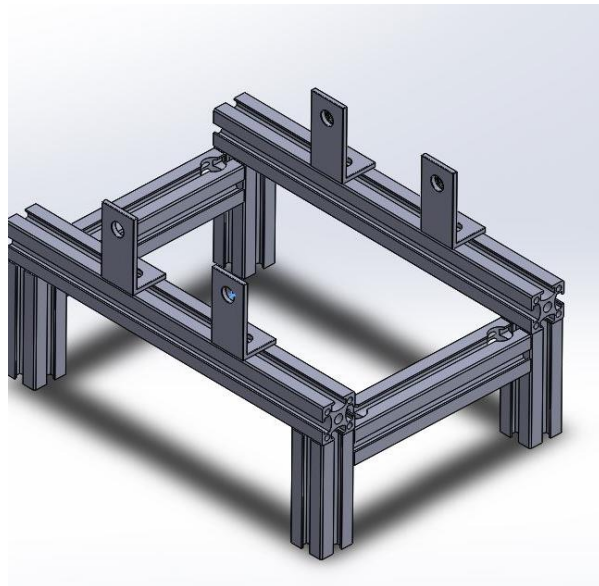


Figure 51. Thruster Stand CAD Model

The stand is designed to be simple and sturdy, made out of x-channel, attached with concealed 90° connectors and straight pins. The stand is large enough to span the opening in the bottom of the vacuum chamber while not being overly complicated or expensive.

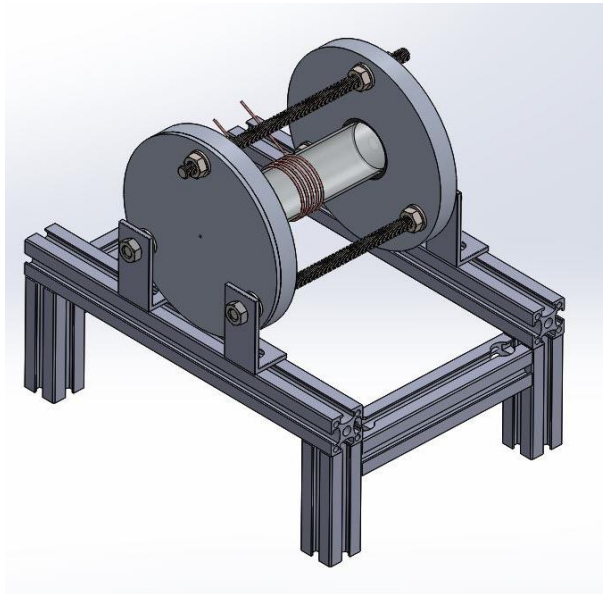


Figure 52. RFET and Thruster Integration

CHAPTER 4: CONCLUSIONS AND RECOMMENDATIONS

4.1 Conclusions

Based on WPI's learning objectives for MQP, the following was achieved:

- *Apply fundamental and disciplinary concepts and methods in ways appropriate to their principal area of study.*

This project used many concepts core to aerospace engineering. There are two subsets of concepts that were utilized, technical and non-technical. They were divided up depending on whether they were concept specific to engineering or concepts general to completing a project.

The technical concepts were focused around fluids and heat transfer as well as structures and manufacturing. In the beginning of the project, two mathematical models were created to describe what was happening inside the thruster. The MATLAB model and the COMSOL models both relied heavily on a solid understanding of fluid flow and heat transfer. Once the conceptual models were created, the actual thruster design and corresponding CAD model relied on a knowledge of stress and structures as well as machining and materials. There were important considerations made concerning the strength of different materials, their melting points as well as force distributions and points of heavy loading.

The non-technical concepts focused on aspects of project and group work which are important to ensuring that the task is completed and done on a budget. The two main skills focused on were organization and budgeting. For the first two thirds of the project, a detailed Gantt Chart was created to help break down the project into smaller manageable goals. This also was used to created deadlines for each aspect of the project, understand the flow of work

and the importance of each aspect. In addition, throughout the entire project, a detailed budget was kept for every item purchased. This was used to ensure that the limited budget of the project was kept to and to assess the importance of each item purchased compared to its cost.

- *Demonstrate Skill and knowledge of current information and technological tools and techniques specific to the professional field of study.*

This project relied on the use of many state of the art pieces of software as well as systems used in the professional field. The mathematical modeling was all done in MATLAB and checked using Microsoft Excel. This was an important tool for performing many iterative calculations quickly and accurately. In addition, another model was created in COMSOL, which is a state of the art piece of software capable of modeling all aspects of the project, from simple heat transfer to more complicated gas ionization. While the software was used nowhere to its full capability, it was still important for understanding design options without ever having to create a physical model. The final piece of software used was Solidworks, which allowed for detailed CAD work to be done and important design changes to be made quickly. It was also used to eventually create the program that would guide the machining of the actual thruster.

This project also worked with two important systems, vacuum technology systems and RF power supplies. Both of these are very important in the fields of aerospace engineering and plasma physics. The project required a basic understanding of RF systems and more importantly, how to use and operate them. A rate-of-rise test was performed to check the vacuum chamber for leaks as it was pumped down. A matching network was also designed for the RF power supply.

- *Use effectively oral, written and visual communication.*

As a team, every other week for the first three terms of the project, presentations about the project background, current progress, issues that had arisen, and problems solved were given. They required the use and design of PowerPoint presentations, conveying technical knowledge to peers who may not have identical backgrounds in the material covered. In addition, weekly check-ins and status reports were due. These focused on communicating what had been achieved in the previous week or term, and ensured that the entire team was working on the same page.

This report also serves to demonstrate the team's written communication skills. It serves as a background to the project for future teams and a reference on RFET thrusters and the different aspects that influence the project.

- *Identify, analyze and solve problems creatively through sustained critical investigation.*

Throughout the project, there were two main problems that required solving as well as one overarching problem which dictated much of the direction of the project. The overarching problem was the lack of information and research about RFET thrusters in general. While it is a topic that has been explored in the past, there are no instruction on how to design and build one. Many different sources had to be compiled to even just get a general idea of scale and gas flow rate. In addition, there were many unknowns in the project that much of the background research glossed over, such as the need and design for an impedance matching network. Solving these problems boiled down to two major issues, machining limitations and matching

network design.

While it was fairly simple to complete a preliminary design for the thruster, when it came time to machine, it became clear that many of the specifications were impossible to extremely difficult to machine. Some of these problems were solved by simple redesigns, such as changing from a collar keeping the O-rings in place to just using a piston seal, while other were more complicated, such as trying to machine a nozzle. While in the end the nozzle had to be removed from the scope of the project, many possibilities were explored, such as less common machining methods or changing materials to graphite.

The matching network also posed many difficulties. The problem boils down to needing to get enough power to the gas to create plasma by matching the impedance. The only problem is that the impedance is unknown, so there is no starting point in which to try and match from. Luckily this was solved when a paper was found outlining impedance of argon, giving the necessary starting point in which to design the system from.

- *Integrate information from multiple sources.*

The first portion of the project, the literature review, consisted solely of compiling information from varying sources and seeing how they all related. The background required researching into plasma physics, vacuum systems and electric propulsion, all of which needed to be integrated into an RFET thruster. Each aspect of the background was necessary for the project, because of the very specific conditions under which the RFET thruster can run. In addition, there was a multidisciplinary aspect to the project, brought in by the RF power supply and impedance matching network. Circuit design and working with RF power is usually more geared towards

electrical engineering and less towards aerospace, but was necessary for this project.

- *Demonstrate an awareness and application of appropriate personal, societal and professional ethical standards.*

All ethical standards were met in the project by way of group interaction and the meeting of deadlines. The team worked well as a group together, dividing up work as needed and asking for assistance when points of confusion arose. In addition, everything written was peer reviewed and edited by all members of the team, ensuring that everything written reflects the team as a whole. There was a strict policy of meeting deadline or informing everyone involved well ahead of time if deadlines needed to be changed. In addition, the team followed the appropriate guidelines for referencing information and acknowledging copyrighted work. These can be seen throughout the entirety of this paper as well as in the bi-weekly presentations given.

- *Practice the skill, diligence and commitment to excellence needed to engage in lifelong learning.*

The team constantly assessed the work of its other members, and was also subject to review by the aerospace faculty and peers. In addition, the scope of the project was reassessed multiple times based on budget and time concerns. The limitations of the project were observed and the following section summarizes where the project should go in the future, the work that was not completed and the parts of the project that could be improved.

4.2 Recommendations for Future Work

The original scope of this project and the final product are very different. Along the way, many problems that were not originally anticipated held up the progress of the project. The following section outlines all of the portions of the project that were not completed as well as recommendations for future work on the project and ways to improve what was accomplished.

First are recommendations concerning the thruster itself. While much of the thruster was completed, it is still missing one important piece, the antenna. Unfortunately due to the lack of time and funding for actually testing the thruster, no work was able to be done on the antenna itself. As of now, the power can reach the vacuum chamber, but there is nothing in place to get the power from the feedthrough to the thruster itself. There needs to be some form of power cable able to withstand the temperature of the plasma and some way to ground the antenna to the chamber itself. In addition, there are a few areas that although designed based on the mathematical modeling, will need redesigning and troubleshooting when the thruster is actually tested. There is a concern about the temperature that the O-rings sealing the quartz tube to the housing will reach and the possibility of melting. There may be need to more heat resistant O-rings or some sort of cooling method to prevent melting. There is also a concern about the quartz tube shattering on high temperature changes or just simply because of how thing it was needed. A thicker walled quartz tube may be necessary.

Once actual testing is able to occur, multiple flow rates and power levels should be tested. There is no data for how low of a power will be capable of producing plasma in the thruster and how much gas flow rate is actually necessary. The theoretical flow rate was set simply because of the limitations of the vacuum chamber, but testing should be done to

determine what is actually necessary and best for the thruster as designed. The other recommendation is to perform optical spectroscopy on the plume of the thruster. This was unfortunately cut from the project because a working thruster was never finished. This will reveal a great deal about the state of the plume, the composition of the gas and any other elements that may be in the plume, either because they were residually in the chamber or because the exhaust is degrading the materials in the thruster itself.

In the future, there should also be a method of actually determining the thrust produced by the thruster. While the optical spectroscopy is useful for understanding the plume, in the end, the goal of a thruster is to understand the thrust produced compared to the power that it draws. This may be a goal for much further in the future.

Because of manufacturing limitations, no nozzle was ever designed for the thruster. It would be beneficial to determine the correct size, material and process for creating one. Many thrusters of this size are tested without nozzles, simply being proof of concepts. It is a difficult problem, due to the small size of the nozzle and the high temperatures which it will reach.

The final area which still needs to be completed is the matching network. While the ground work has been done to design one, it was never built. The first step should be to build the network based on the specifications given in section 3.3, but from there, extensive troubleshooting will be necessary. There is no proof that the designed network will allow an appreciable amount of power through to the plasma, so it may need to be redesigned with different capacitors. Once it is built, the thruster should be tested first without the matching network to see how much power gets reflected back to the supply. From there, it should be tested with the network, so that impedance plots can be created. This will allow it to be easily

tuned or adjusted in the future. It would be beneficial to try a range of inductors in the matching network to achieve the closest match and most power transmitted.

REFERENCES

- ¹Charles, C., et al., "Nanosecond Optical Imaging Spectroscopy of an Electrothermal Radiofrequency Plasma Thruster Plume," *Applied Physics Letters*, 2013, pp. 1-5.
- ²Ahedo, Eduardo, "Plasma for Space Propulsion," *IOP Science*, 2011, pp. 1-14.
- ³Greig, A., et al., "Direct Measurement of Neutral Gas Heating in a Radio-Frequency Electrothermal Plasma Micro-Thruster," *Applied Physics Letters*, 2013, pp. 4-5.
- ⁴Hopkins, Jeffrey R., Micci, Michael M. and Bilen, Sven G, "Design and Testing of a Low Power Radio-Frequency Electrothermal Thruster" Presented at the 31st International Electric Propulsion Conference, 2009, pp. 1-5.
- ⁵Boswell, Rod, et al, "Plasma Expansion From a Radio Frequency Microdischarge 11," *IEEE Transactions on Plasma Science*, Vol. 39, 2011, pp. 2512-2514.
- ⁶Zhu, Xi-Ming and Pu, Yi-Kang, "Using OES to Determine Electron Temperature and Density in Low-Pressure Nitrogen and Argon Plasmas" *Plasma Sources Science and Technology*, Vol. 17, 2008, p. 6.
- ⁷Moore, John H., Davis, Christopher C. and Coplan, Michael A, "Building Scientific Apparatus 1st," Perseus Books, Cambridge, 1983.
- ⁸Sharp, Jeremy, "Plasma Monitoring with the HR2000+ High Resolution Spectrometer," *The Ocean Optics Applications Blog*, 2012, p. 1.
- ⁹Charles, C., et al. "Nanosecond Optical Imaging Spectroscopy of an Electrothermal Radiofrequency Plasma Thruster Plume," *Applied Physics Letters*, Vol. 103, 2013, p. 1.
- ¹⁰Casper, Budtz-Jorgensen V, "Studies of Electrical Plasma Discharges," Aarhus University, Aarhus, 2001.
- ¹¹Zaplotnik, R., Vesel, A. and Mozetic, M, "Transition from E to H Mode in Inductively Coupled Oxygen Plasma: Hysteresis and the Behavior of Oxygen Atom Density," Josef Stefan Institute Ljubljana, 2011.
- ¹²Lee, Hyo-Chang, Kim, Dong-Hwan and Chung, Chin-Wook, "Discharge Mode Transition and Hysteresis in Inductively Coupled Plasmas," *Applied Physics Letters*, Vol. 102, 2013, pp. 1-3.
- ¹³Fei, Gao, et al., "Spatial Variation Behaviors of Argon Inductively Coupled Plasma During Discharge Mode Transition," *China Physics B*, Vol. 21, 2012, pp. 1-3.
- ¹⁴Gonzalez, Luis, et al. "Optical Emission Study of a Pulsed Plasma Thruster JB3-PPT2," Worcester Polytechnic Institute, Worcester, 2014.
- ¹⁵Jahn, Robert G, "Physics of Electric Propulsion," McGraw-Hill Book Company, New York, 1968.
- ¹⁶Schmidt, Wayne. "Electric Rocket Engine Basics.," *Wayne's This and That*.
<http://www.waynesthisandthat.com/ep2.htm>, [cited 15 November 2014]
- ¹⁷Kim, Yongho, "Low Temperature Atmospheric Pressure Plasmas: Physics, Diagnostics, and Applications," *ICOPS/BEAMS 2014*, 2014. <http://www.ece.unm.edu/icops-beams2014/lowtemp.html>. [Cited March 21 2015.]
- ¹⁸Starck, Axel von, Muehlbauer, Alfred and Kramer, Carl. Frequency Bands. "Handbook of Thermoprocessing Technologies," Essen, Vulkan-Verlag GmbH, 2015, p. 197.
- ¹⁹Plasma Processing, "Ciência, Tecnologia e Inovação,"
http://www.plasma.inpe.br/LAP_Portal/LAP_Site/Text/Plasma_Processing.htm. [Cited March 15 2015]
- ²⁰Goebel, Dan M. and Katz, Ira. "Fundamentals of Electric Propulsion: Ion and Hall Thrusters. s.l," NASA, 2008.
- ²¹Ahedo, Et Al, "Plasma Dynamics in a Helicon Thruster," *EDP Sciences*, 2013, Vol. Progress in Propulsion Physics.
- ²²Technical Glass Products, Inc. Product Catalog, http://www.technicalglass.com/downloads/TGP_2010_Catalog.pdf. [Cited March 20 2015.]
- ²³Lafleur, T, et al., "Direct thrust measurements and modelling of a radio-frequency expanding plasma," AIP Publishing, 2011, Vol. Physics of Plasmas.
- ²⁴"The ARRL handbook for radio communications," 80, Newington, AARL, 2002, Impedance Matching Networks. p. 1547-1470.
- ²⁵Vaghela, N, "Application Note - RF (13.56) Impedance Matching," Farmingham, Huettinger Electronic Inc.
- ²⁶Long, S, "ECE145A/ECE 218A Notes Set #5," Santa Barbara, UCSB ECE Department, 2007.
- ²⁷Allard, Robert, et al., "Creation of an Inductively Coupled Plasma," Fort Collins, Department of Electrical and Computer Engineering, Colorado State University, 2007.
- ²⁸Colpo, Pascal, Ernst, Roland and Rossi, "Determination of the equivalent circuit of inductively coupled," *Journal of Applied Physics*, Vol. 85, 1998

- ²⁹ [Anonymous]. Parker Hannifin Corporation. Parker O-Ring Handbook, [online] 2007, https://www.parker.com/literature/O-Ring_Handbook.pdf. Accessed March 5, 2015.
- ³⁰ [Anonymous]. Swagelok, Product Catalog, 2013. [online] http://www.swagelok.com/tools/download_pdf.aspx. Accessed March 5, 2015.
- ³¹ Person Communication with Dr. Lynn Olson, at Busek Co. Inc
- ³² Choueiri, Edgar and Polzin, Kurt. "Faraday Acceleration with Radio-frequency Assisted Discharge (FARAD)," AIAA, 2004-3940, 2004.
- ³³ [Anonymous]. RF Parts Company. Product Listing. [online] 2015. Available from: www.rfparts.com. Accessed 3/12/15
- ³⁴ [Anonymous]. McMaster Carr. Product Listing. [online] 2015. www.mcmaster.com.
- ³⁵ [Anonymous]. Coil Winding Specialists. Product Listing. [online] 2015. www.coilws.com.
- ³⁶ [Anonymous]. Summit Racing Equipment. Product Listing. [online] 2015. www.summitracing.com.
- ³⁷ [Anonymous]. Pasternack. Product Listing. [online] 2015. www.pasternack.com.
- ³⁸ [Anonymous]. Ideal Vacuum Systems. Product Listing. [online] 2015. www.pchemlabs.com.
- ³⁹ [Anonymous]. Vacuum Research Corporation. Product Listing. [online] 2015. www.vacuumresearchcorp.com.
- ⁴⁰ Bejan, Adrian, "Heat Transfer," John Wiley & Sons, New York, 1993.

APPENDICES

Appendix A

0-D MATLAB Code

```
%% Initial Calculations
%   These are the initial calculations off of which we will base our
%   initial designs and tests.
clear all
clc
%% Import Isentropic Flow Table
isen_flow = load('Isentropic_Flow_Table.txt');
% expansion ration -> 48.2403
%% Controlable Values
exp_ratio = 48.2403; %input('What is your Expansion Ration? '); Expansion
Ratio
e_row = isen_flow(:,3);
isen_row = find(e_row==exp_ratio);
P_row = isen_flow(:,4);
P_ratio = P_row(isen_row);
P_b = 0.1; % Back Pressure, Pascals
Q_dot = 1:500; % Input Power input, Watts
m_dot = 0.5/1000000; % Mass Flow Rate, kg/s
Length = 0.127; % Length of Quartz Tube, m
Diameter = 0.015; % Inner Diameter of Quartz Tube, m
diameter_throat = input('What is the diameter of the throat? (in mm) ');
Area_throat = pi*(diameter_throat/1000/2)^2; % Area of Throat, m^2
Area_exit = Area_throat*exp_ratio; % Throat Exit Area, m^2
%% Guess Calculations
R_c = 8.3144621; % Universal Gas Constant, kJ/K/mol
MW_AR = 39.948/1000; % Molecular Weight of Argon, kg/mol
MW_e = 5.4857990946e-7; % Molecular Weight of Electron, kg/mol
C_p_AR = 20.785;
C_p_e = 20.785;
T_in = 298; % Room Temperature, Kelvin
k = 5/3; % Specific Heat Ratio
h_fd = 1520600; % Ionization Enthalpy first order Argon J/mol
C_const = 0.0667;
theta_i = 1.8335e5; % K
e = 0.001; % emissivity of Chamber
surf_area = 2*pi*Diameter/2*Length+2*pi*(Diameter/2)^2; % Inner Surface Area
of Chamber
sigma = 5.67e-08; % Stefan-Boltzmann Constant, J/s/m^2/K^4
for i = 1:500
    c = 0;
    T = zeros(500,1);
    P = zeros(500,1);
    tol = 1;
    T(1) = 300;
    P(1) =
(m_dot/Area_throat)*(1/k)*sqrt((MW_AR*T(1))/(k*((2/(k+1))^(k+1)/(k-1)))));
    while tol > 0.0001
        c = c+1;
        A = C_const*(T(c)^(5/2))/P(c)*exp(-theta_i/T(c));
        phi_deg = sqrt(A/(1+A)); % Degree of Ionization
        n_AR = (1-phi_deg)/(1+phi_deg); % Moles of Argon
```

```

n_ARi = phi_deg/(1+phi_deg); % Moles of Argon Ion
n_e = n_ARi; % Moles of Electrons
Z = Q_dot(i)*MW_AR/m_dot;
B = e*sigma*surf_area*MW_AR/m_dot;
C = h_fd*n_ARi;
D = C_p_e*(1+n_e);
T(c+1)= fsolve(@(T_calc) (Z-T_calc^4*B-C)/D-T_calc+298,T(c));
P(c+1) = (m_dot/Area_throat)*sqrt((MW_AR*T(c+1))/(k*((2/(k+1))^(...
(k+1)/(k-1))))); % Actual Stag Press, Pascals
tol = abs(T(c)-T(c+1));
end
n_ARi1(i) = n_ARi;
T_01(i) = T(c+1);
P_01(i) =
(m_dot/Area_throat)*sqrt((1000*R_c/MW_AR*k*T_01(i))/(k*((2/(k+1))^(...
(k+1)/(k-1)))))/1000;
P_e1(i) = P_ratio*P_01(i);
u_e1(i) = sqrt(2000*R_c/MW_AR*k/(k-1)*T_01(i)*(1-(P_ratio)^((k-1)/k)));
I_sp1(i) = u_e1(i)/9.81;
F1(i) = m_dot*u_e1(i)+(P_e1(i)-P_b)*Area_exit;
end
m_dot = 1/1000000;
for i = 1:500
c = 0;
T = zeros(500,1);
P = zeros(500,1);
tol = 1;
T(1) = 300;
P(1) =
(m_dot/Area_throat)*(1/k)*sqrt((MW_AR*T(1))/(k*((2/(k+1))^(k+1)/(k-1)))));
while tol > 0.0001
c = c+1;
A = C_const*(T(c)^(5/2))/P(c)*exp(-theta_i/T(c));
phi_deg = sqrt(A/(1+A)); % Degree of Ionization
n_AR = (1-phi_deg)/(1+phi_deg); % Moles of Argon
n_ARi = phi_deg/(1+phi_deg); % Moles of Argon Ion
n_e = n_ARi; % Moles of Electrons
Z = Q_dot(i)*MW_AR/m_dot;
B = e*sigma*surf_area*MW_AR/m_dot;
C = h_fd*n_ARi;
D = C_p_e*(1+n_e);
T(c+1)= fsolve(@(T_calc) (Z-T_calc^4*B-C)/D-T_calc+298,T(c));
P(c+1) = (m_dot/Area_throat)*sqrt((MW_AR*T(c+1))/(k*((2/(k+1))^(...
(k+1)/(k-1))))); % Actual Stag Press, Pascals
tol = abs(T(c)-T(c+1));
end
n_ARi2(i) = n_ARi;
T_02(i) = T(c+1);
P_02(i) =
(m_dot/Area_throat)*sqrt((1000*R_c/MW_AR*k*T_02(i))/(k*((2/(k+1))^(...
(k+1)/(k-1)))))/1000;
P_e2(i) = P_ratio*P_02(i);
u_e2(i) = sqrt(2000*R_c/MW_AR*k/(k-1)*T_02(i)*(1-(P_ratio)^((k-1)/k)));
I_sp2(i) = u_e2(i)/9.81;
F2(i) = m_dot*u_e2(i)+(P_e2(i)-P_b)*Area_exit;
end
m_dot = 1.5/1000000;

```

```

for i = 1:500
    c = 0;
    T = zeros(500,1);
    P = zeros(500,1);
    tol = 1;
    T(1) = 300;
    P(1) =
(m_dot/Area_throat)*(1/k)*sqrt((MW_AR*T(1))/(k*((2/(k+1))^(k+1)/(k-1)))));
    while tol > 0.0001
        c = c+1;
        A = C_const*(T(c)^(5/2))/P(c)*exp(-theta_i/T(c));
        phi_deg = sqrt(A/(1+A)); % Degree of Ionization
        n_AR = (1-phi_deg)/(1+phi_deg); % Moles of Argon
        n_ARi = phi_deg/(1+phi_deg); % Moles of Argon Ion
        n_e = n_ARi; % Moles of Electrons
        Z = Q_dot(i)*MW_AR/m_dot;
        B = e*sigma*surf_area*MW_AR/m_dot;
        C = h_fd*n_ARi;
        D = C_p_e*(1+n_e);
        T(c+1) = fsolve(@(T_calc) (Z-T_calc^4*B-C)/D-T_calc+298,T(c));
        P(c+1) = (m_dot/Area_throat)*sqrt((MW_AR*T(c+1))/(k*((2/(k+1))^(...
            (k+1)/(k-1))))); % Actual Stag Press, Pascals
        tol = abs(T(c)-T(c+1));
    end
    n_ARi3(i) = n_ARi;
    T_03(i) = T(c+1);
    P_03(i) =
(m_dot/Area_throat)*sqrt((1000*R_c/MW_AR*k*T_03(i))/(k*((2/(k+1))^(...
        (k+1)/(k-1)))))/1000;
    P_e3(i) = P_ratio*P_03(i);
    u_e3(i) = sqrt(2000*R_c/MW_AR*k/(k-1)*T_03(i)*(1-(P_ratio)^((k-1)/k)));
    I_sp3(i) = u_e3(i)/9.81;
    F3(i) = m_dot*u_e3(i)+(P_e3(i)-P_b)*Area_exit;
end
figure
subplot(2,2,1)
plot(Q_dot,T_01,Q_dot,T_02,Q_dot,T_03)
title('Chamber Temperature vs RF Power','FontSize',16)
xlabel('RF Power Generator (Watts)','FontSize',12)
ylabel('Chamber Temperature (Kelvin)','FontSize',12)
legend('m_dot = 0.5 mg/s','m_dot = 1 mg/s','m_dot = 1.5 mg/s')
subplot(2,2,2)
plot(Q_dot,P_01,Q_dot,P_02,Q_dot,P_03)
title('Chamber Pressure vs RF Power','FontSize',16)
xlabel('RF Power Generator (Watts)','FontSize',12)
ylabel('Chamber Pressure (kPa)','FontSize',12)
legend('m_dot = 0.5 mg/s','m_dot = 1 mg/s','m_dot = 1.5 mg/s')
subplot(2,2,3)
plot(Q_dot,I_sp1,Q_dot,I_sp2,Q_dot,I_sp3)
title('Specific Impulse vs RF Power','FontSize',16)
xlabel('RF Power Generator (Watts)','FontSize',12)
ylabel('Specific Impulse (sec)','FontSize',12)
legend('m_dot = 0.5 mg/s','m_dot = 1 mg/s','m_dot = 1.5 mg/s')
subplot(2,2,4)
plot(Q_dot,1000*F1,Q_dot,1000*F2,Q_dot,1000*F3)
title('Thrust vs RF Power','FontSize',16)
xlabel('RF Power Generator (Watts)','FontSize',12)

```



```
ylabel('Thrust (mN)', 'FontSize', 12)  
legend('m_dot = 0.5 mg/s', 'm_dot = 1 mg/s', 'm_dot = 1.5 mg/s')
```